Study on heterogeneous nucleation of colloidal crystals: the effect of interfacial free energy on nucleation process

博士論文

Study on heterogeneous nucleation of colloidal crystals: the effect of interfacial free energy on nucleation process

（コロイド結晶の不均質核形成についての研究—核形成プロセスに対する界面自由エネルギーの効果—）

Suxia Guo

郭 素霞

平成 30 年

Contents

Chapter 1 Introduction

This study investigates the nucleation process using colloidal crystals. The understanding of process is very important for various fields including metallurgy, physics, and biology. In this chapter, studies on the nucleation process and colloidal crystals are reviewed and the aim of this study is discussed.

1.1 Nucleation

Nucleation is an important phenomenon not only in materials science but also in chemistry and physics. The crystallization process is a central topic in materials science, comprising both nucleation and growth processes. The nucleation process is an initial process in phase transition. Nucleation is defined as an irreversible formation of a nucleus of the new phase, where a small quantity of atoms, ions, or molecules forms a new structure in a small region of a crystal from the solution, liquid, vapor, or solid phase. Nucleation can be classified as homogeneous and heterogeneous nucleation. The nuclei of the new phase formed uniformly throughout the parent phase represent homogeneous nucleation, while those formed preferentially at the walls of the container, impurities, grain boundaries, dislocations, etc., indicate heterogeneous nucleation.

1.1.1 Nucleation phenomenon in nature

The nucleation process universally occurs when a new phase is formed. There are various examples of nucleation, such as in ice, cloud, snow, and rainfall formation; in the origin of life, such as the organic and inorganic proteins; and in mineral crystallization such as volcanic eruptions and earthquakes. The initiation of neuro-degenerative diseases and the formation of black holes are also produced

by the nucleation process [1]. Heterogeneous nucleation occurs more often than homogeneous nucleation in nature. The reason for this will be described in the next section from thermodynamic viewpoint. There are some typical examples of heterogeneous nucleation in life, such as the formation of carbon dioxide bubbles and the growth of sugar crystals on a string.

The nucleation process occurs not only in the atomic or molecular crystal but also in large building blocks. Nucleation also occurs in macromolecular systems such as proteins whose molecular size is on the order of several nanometers. The authors in [2] observed the nucleation of 2D glucose isomerase crystals on a substrate and found that the nucleation process was similar to that of the atomic system. Beyond the typical example, on the kilometer scale, the occurrence of an earthquake was indicated to be a nucleation process by near-source observations [3, 4]. The submicron size of the colloidal particle also shows the nucleation process. It is known that colloidal particles display a phase transition similar to that of the atomic system. Russo and Tanaka investigated the nucleation behavior of the colloidal system [5, 6], which has been applied to study the kinetics of phase transition [7, 8].

1.1.2 Classical nucleation theory (CNT)

CNT is a well-known theoretical model used to understand the nucleation phenomenon, which stems from the studies of Volmer and Weber [9], Becker and Döring [10], and Frenkel [11]. This model presents the condensation of supersaturated vapors to the liquid phase and can also be applied to crystallization from solutions and melts. The change in Gibbs free energy of the system (ΔG) during nucleation is the sum of decrease in volume energy (ΔG_v), which arises from the gain of the chemical potential difference, and the increase in the

interfacial energy (ΔG_s) induced by the formation of a surface. The nucleation process depends on the competition between ΔG_v and ΔG_s. Thus, ΔG for a spherical nucleus with radius r is given by

$$\Delta G(r) = -\frac{4\pi r^3}{3v_1}\Delta\mu + 4\pi r^2 \cdot \sigma \tag{1.1}$$

where $\Delta\mu$ is the chemical potential difference between the liquid and solid, σ is the interfacial energy between the liquid and solid per unit area, and v_1 is the molecular volume of the liquid. Based on eq. 1.1, the change in ΔG for nucleation, as a function of the radius of the nuclei, r, is shown in Figure 1.1. As seen in Figure 1.1, there is a maximum value of ΔG, the critical Gibbs free energy change, ΔG^*, which corresponds to the critical size, r^*. When the size of the nuclei is less than r^*, ΔG increases with r. Thus, the clusters will gradually dissolve. As r increases beyond r^*, the decrease in ΔG leads to the formation of the nuclei.

Based on the above discussion, the thermodynamic perspective of heterogeneous nucleation is described. The free energy needed for heterogeneous nucleation is expressed as [12]

$$\Delta G_{\text{heterogeneous}} = \Delta G_{\text{homogeneous}} * f(\theta) \tag{1.2}$$

where $f(\theta) = \frac{(1-\cos\theta)^2(2+\cos\theta)}{4}$, where θ is the contact angle of the nuclei and the foreign substance during the heterogeneous nucleation process, as shown in Fig.1.2 (a). The ΔG for heterogeneous nucleation compared to that for homogeneous nucleation is shown in Figure 1.2(b). The r^* for heterogeneous nucleation is the same as that for homogeneous nucleation, whereas the critical Gibbs free energy change for heterogeneous nucleation, $\Delta G_{\text{heterogeneous}}{}^*$, is less than that for homogeneous nucleation, $\Delta G_{\text{homogeneous}}{}^*$. Owing to the smaller ΔG value, heterogeneous nucleation occurs more frequently in nature than homogeneous

nucleation.

Here, the limitations of applying the classical nucleation theory are discussed. We make the following assumptions in CNT, to simplify the process description: small clusters have the same properties as those of the bulk material, the shape of the nucleus is spherical, the cluster grows by the addition of one monomer at a time (Figure 1.1(a)), the interfacial energy is independent of the size, and the process is in equilibrium [13, 14]. These assumptions limit the application of CNT. For instance, the nucleation rate of water vapor in the presence of argon inferred from the expansion chamber with a temperature control system is 1–2 orders of magnitude lower than that of the water vapor inferred from CNT predication [15]. Although CNT has developed since its introduction by Gibbs in the 1870s [16, 17], the quantitative nucleation kinetics are yet to be fully understood.

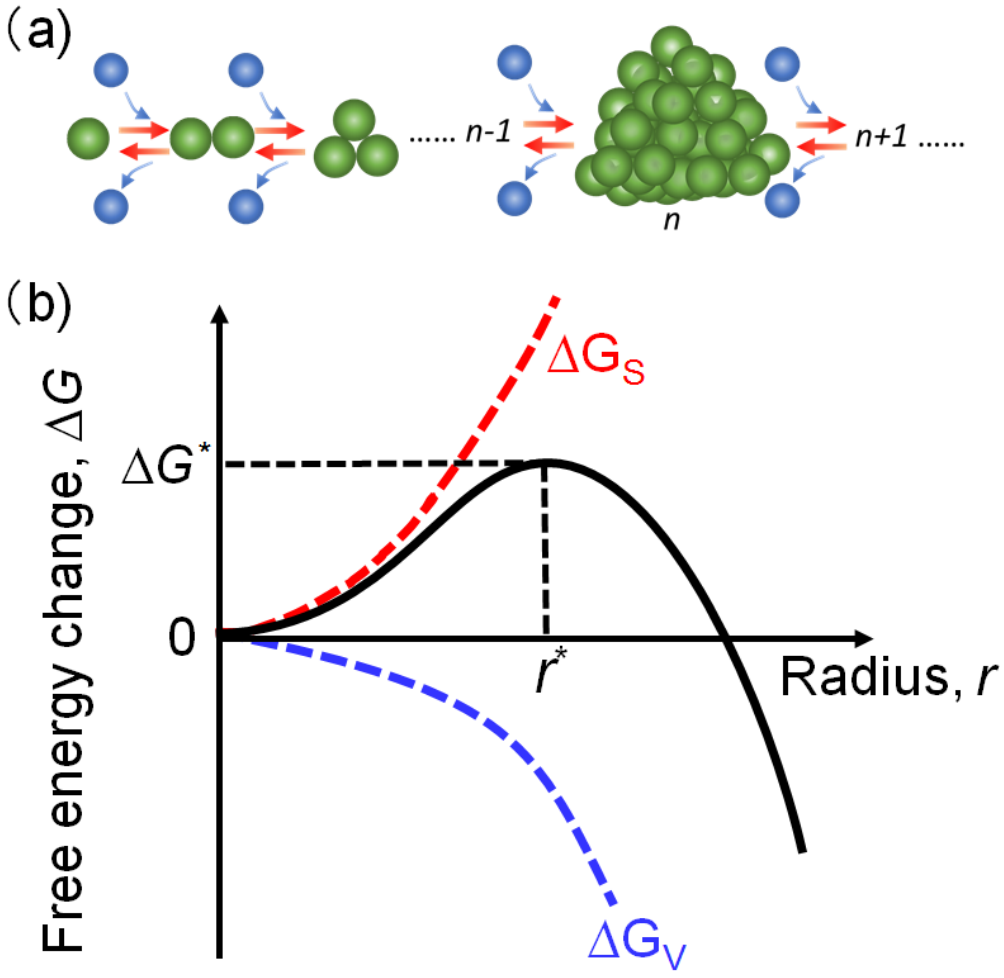

Figure 1.1 Classical nucleation theory: (a) Growth of nuclei—Only one atom is incorporated at a time; *n* is the number of atoms, the green sphere is the atom of a growing cluster, the blue sphere is a free atom. (b) Change in Gibbs free energy (ΔG) for nucleation as a function of the radius of nuclei, *r*, according to the CNT.

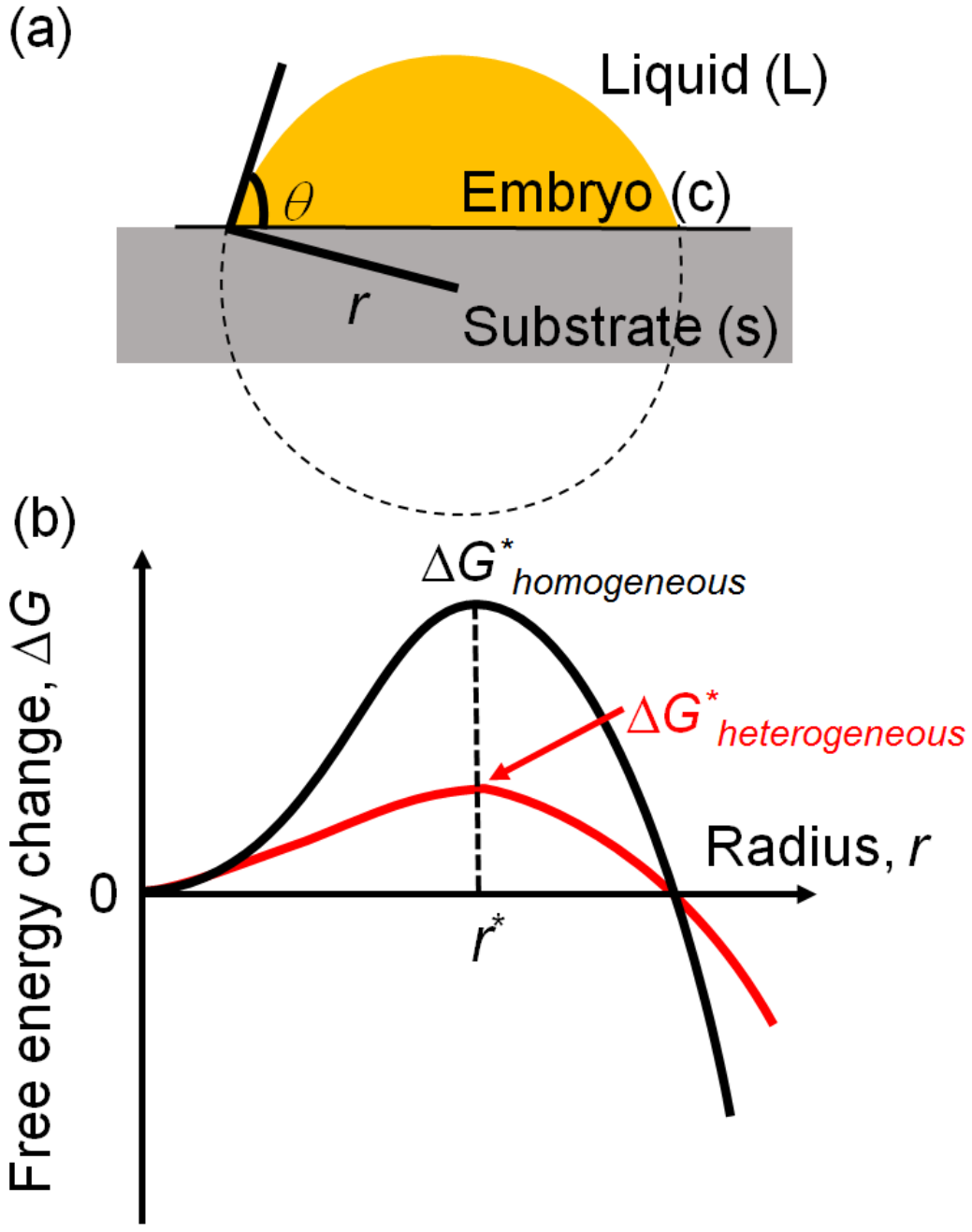

Figure 1.2 ΔG^* of heterogeneous nucleation is less than that of homogeneous nucleation. (a) The equilibrium state of the nuclei with a radius r on a flat substrate. θ is the contact angle of the embryo and the foreign substrate. (b) Schematic of ΔG curves for homogeneous and heterogeneous nucleation as a function of r.

1.2 Colloidal crystals

The materials employed in this study are colloidal crystals, which are monodispersed colloids in which colloidal particles are arranged orderly. They have attracted much attention due to their unique properties. After reviewing the applications of colloidal crystals, the nucleation process of colloidal crystals is described.

1.2.1 Colloids and colloidal crystals

The term colloid is a state of submicron particles, with sizes ranging from 1 nm to 1 μm, dispersed in a solid, liquid, or gas medium according to IUPAC's definition [18]. A colloid comprises colloidal particles and the dispersing medium. Colloids are ubiquitous in everyday life. Some examples include milk, smog, fog, paints, muddy water, and cosmetics. For instance, tiny grains of sand, silt, and clay dispersed in water form muddy water. Fog refers to the dispersion of water droplets in air. Milk is an emulsion of liquid butterfat globules suspended in a water-based solution.

A colloidal crystal has the structure of a highly ordered arrangement of particles, which is analogous to a normal crystal arrayed by atoms or molecules [19]. The structure of colloidal crystals is 2D (i.e., monolayer), which is only one particle high, and 3D (i.e., multilayer), which extends along all three spatial coordinates. Figure 1.3 shows 3D polystyrene colloidal crystals, with a face-centered cubic (fcc) structure [20].

In general, colloidal crystals exist in nature and can be artificially synthesized from polymer spheres. For instance, some viruses for animal or plant diseases are colloidal crystals [21, 22]. Stanley discovered the tobacco mosaic virus in 1935, which was identified to be naturally monodispersed by Bernal and

Fankuchen in 1941. These virus particles were assembled into crystals after being concentrated by centrifuging from dilute water suspensions, and then examined by light diffraction methods. Williams and Smith reported that a crystalline order was observed in suspensions of Tipula virus by a high-magnification light microscope [23]. A typical example of a natural colloidal crystal is opal, whose regular order of the spherical silica particles was revealed by Darragh et al., where sparkles with flecks of pure spectral color were observed due to the diffraction of visible light [24, 25].

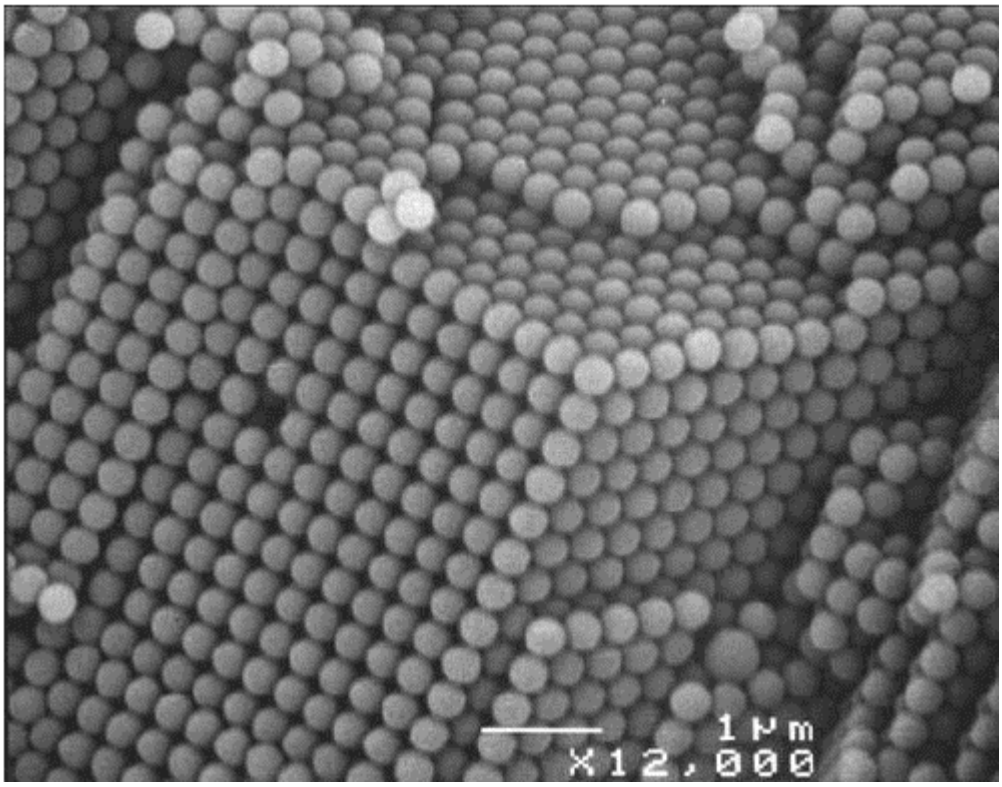

Figure 1.3 Scanning electron micrograph of a polystyrene colloidal crystal. Reprinted with permission from Reference [20] © Kluwer Academic Publishers 2004.

Colloidal crystals exhibit some unique features. Bragg scattering of visible light by a colloidal crystal occurs because the lattice constant of the colloidal crystal is comparable with the wavelength of visible light. Colloidal particles are characterized by observable Brownian motion from the viewpoint of physics [26]. Brownian movement arises because each particle in the colloidal solution has kinetic energy. The movement of colloidal particles in a medium is analogous to the diffusion of atoms. The crystallization process of colloidal particles shows a phase transition analogous to that of the atomic system [27]. Therefore, they have attracted much interest in various applications such as the optical field, chemical engineering, and materials science. These will be introduced in detail in the next section.

1.2.2 Applications of Colloidal Crystals

There are diverse applications of colloidal crystals, and the photonic crystal is a typical one. The photonic crystal can control the propagation of electromagnetic waves, which are induced by a periodic structure composed of two different refractive indexes in the assembly structure [28]. It is similar to the electrons in the semiconductor. Colloidal crystals are the most promising materials for low-cost production of 2D and 3D photonic crystals. By utilizing the unique photonic feature of colloidal crystals, they can be applied to optical waveguides [29]. The laser beam focused on the colloidal crystal microring is guided by a regularly arranged structure due to its strong photoluminescence. Colloidal crystals are also applied to biochemical sensors [30, 31]. A polystyrene colloidal crystal is placed on the surface of a contact lens, which selectively filters electromagnetic waves of certain frequencies according to Bragg's law [30]. "Colloidal lithography" has recently attracted much interest for its application to

photolithography [32–35] and templates for the epitaxial growth of colloidal crystals [36, 37]. To produce surface patterning, 2D colloidal crystals are utilized as masks or templates for the processes of evaporation [35], deposition [38], etching [39], and imprinting [40]. In addition, colloidal crystals have been used as a model system for phase transitions in atomic systems [41]. They can be applied to extreme experimental conditions such as high pressure, high temperature, and short processing time, which are difficult to observe directly in an atomic system. The colloidal system is easily accessible for observing such transitions, because the typical length and time scales can be monitored using an optical microscope.

1.2.3 Colloidal system as a model for atomic systems

As mentioned in the last section, since colloidal crystals possess unique features such as Brownian motion, large size, and tunable interaction, colloidal crystals have attracted much interest for fundamental studies, as they are a promising model for phase transitions in atomic and molecular systems. Following are the advantages of the colloidal system as a model [42–45]. First, the size of the colloidal particles is larger than that of atoms or molecules, which enables individual particles and their spatial arrangements to be visualized directly by an optical microscope. Second, the diffusion of colloidal particles is slower by several orders of magnitude than that of atoms. The long characteristic time of colloids makes it easy to facilitate *in situ* observations in real time. Also, colloidal particles exhibit Brownian motion; when their volume fraction in solutions exceeds a certain level, they exhibit phase transition, such as gas, liquid, or solid. This behavior is analogous to that of atomic systems. In addition, the interactions between colloidal particles can be tailored from repulsive to attractive, which makes it possible to model colloidal suspensions of different system types.

These advantages make colloids a suitable model system to investigate dynamic processes and phase transitions such as glass formation [46], crystal nucleation [47], and epitaxial growth [48] with a single-particle resolution, which provides a good insight into the phenomena that are difficult to experimentally address in atomic systems.

1.3 Development of nucleation study

The control of nucleation is critical for manipulating the number, size, perfection, and other characteristics of crystals [49]. CNT, as a basic theoretical framework, is employed to investigate the nucleation process, and was developed a long time ago, as mentioned in section 1.1.2. It was derived based on several major assumptions, which simply describe the nucleation process but restrict its application simultaneously. Some shortcomings of CNT are discussed here. For instance, CNT cannot predict the absolute nucleation rate if the pre-exponential factor in the kinetic equations remains unknown [50–54]. In the nucleation process of stoichiometric silicate glasses ($Li_2O \cdot 2SiO_2$ and $Na_2O \cdot 2CaO \cdot 3SiO_2$), the movement of clusters was ignored, but the pre-exponential factor was affected by molecular mobility. This assumption led to a significant deviation of the theoretical pre-exponential factor from the experimental one [55]. There is a debate on whether small clusters can be considered to have the same properties as the bulk material. It was reported that the properties of a critical nucleus were significantly different from those of the eventually formed stable bulk phase [56]. Although many researchers have studied the fundamental aspects of the nucleation process by CNT, the nucleation rate is still unpredictable [57]. This stimulates the development of theoretical methods beyond the assumptions of CNT.

Recently, various nucleation processes that cannot be explained by CNT

have been reported, such as two-step nucleation and multi-step nucleation via metastable state in various substances [61–65]. Many factors affect the nucleation process, whose mutual effect leads to a wide variety of dynamic pathways in the formation of the nuclei, as shown in Figure 1.4. The various pathways include the single-step nucleation described by CNT (Figure 1.4a), the two-step nucleation of protein described by the formation of a metastable bulk phase (Figure 1.4b), or the multi-step colloidal nucleation via the appearance of metastable phases (Figure 1.4c).

To a large extent, the development of experimental and simulation techniques such as *in situ* TEM [58] and atomic force microscopy (AFM) [59] allows researchers to investigate the nucleation process in more detail on the length and time scales, which was previously unattainable. Thus far, the understanding of crystal nucleation is far from sufficient because the process is largely unknown from molecular viewpoint. Hence, computational approaches simulate the process of cluster formation and particle assembly using molecular dynamics (MD) simulations [60], which helps in the understanding of nucleation at the nanometer scale. However, the experimental investigation of nucleation is difficult and still a challenge for almost all systems. Since the colloidal system is an excellent model to study phase transition, researchers have applied it to the nucleation study.

In the colloidal system, several studies focusing on the nucleation process have been reported. For instance, homogeneous nucleation was investigated in a hard sphere system [66–68], where the nucleation rate of the hard spheres as a function of volume fraction and the detailed structure of critical nuclei were examined. Heterogeneous nucleation has also been studied. Colloidal crystals nucleate much faster on substrates than in the bulk via homogeneous nucleation.

The ΔG for nucleation on the wall was measured to be two orders of magnitude lower than that for homogeneous nucleation by simulation [69]. Zhang and Liu studied the classical nucleation process of charged polystyrene spheres on a cover glass, in which nucleation is driven by an applied alternating electric current [70]. They also observed multi-step nucleation via an amorphous precursor [64]. Therefore, in distinct materials, nucleation can undergo the classical or non-classical nucleation pathway. Even in the same material, the formation of nuclei shows different pathways due to the interplay of thermodynamics and the dynamics of particles. What determines the nucleation pathway to be followed in the colloidal system remains unclear. The understanding of the mechanism of nucleation still requires investigation.

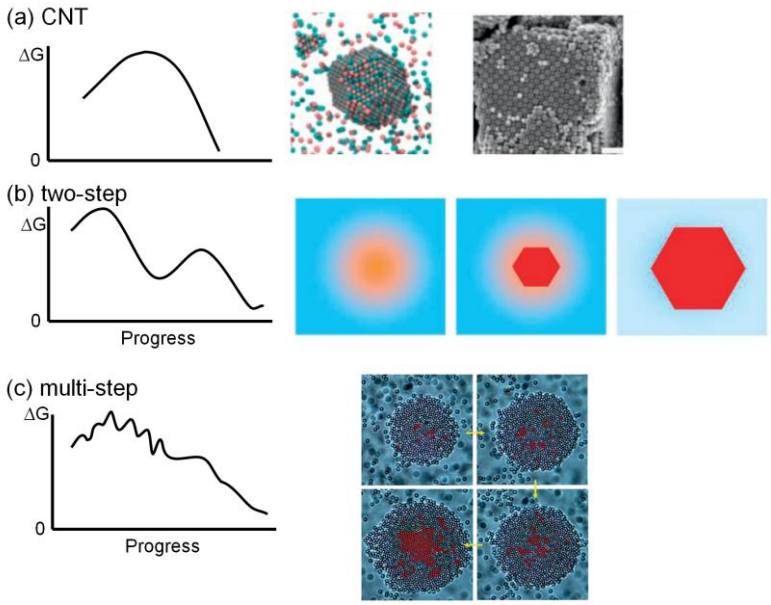

Figure 1.4 Possible pathways and free-energy landscape. (a) Classical nucleation overcoming a smooth barrier (left) for DNA-functionalized nanocubes (green) and nanospheres (orange). This is portrayed by MD simulations (middle). Reproduced with permission from Reference [61]. © 2013, Springer Nature. A scanning electron microscope image of the formed colloidal crystal with a cubic lattice isostructural to NaCl is shown on the right-hand side; Reproduced with permission from Reference [62]. the scale bar is 200 nm. (b) Nucleation via the formation of a metastable bulk phase. Two-step nucleation is typically recognized in protein systems. The crystal phase (red) is nucleated in a dense liquid phase (yellow) formed in a dilute liquid phase (blue). Reproduced with permission from Reference [63] © 1997, The American Association for the Advancement of Science. (c) Nucleation over a barrier with several local minima. Multi-step crystallization observed in a 2D colloidal system. The crystal-like particles defined by $\langle|\psi_6|\rangle >$ 0.8 are highlighted in red (where ψ_6 is a local 2D bond-order parameter). Readapted with permission from [64]. Copyright (2007) American Chemical Society.

1.4 Interfacial free energy

As previously described, heterogeneous nucleation on a substrate is a common mode of crystallization in industry as well as in nature, based on thermodynamics. Thus, the substrate plays a crucial role in the nucleation process. Many efforts have been devoted to studying the effect of the substrate on the nucleation process, e.g., the effect of substrate temperature [71] and the surface structure of the substrate [72].

The substrate also plays a vital role in the nucleation of colloidal crystals [73–75]. Several studies on the effect of substrates have been conducted. For instance, it was reported that the presence of a smooth hard wall drastically lowered the nucleation barrier of colloidal crystals in a hard sphere system, where the critical Gibbs free energy for nucleation on the wall was lower than that for homogeneous nucleation by about two orders of magnitude [69]. Arai et al. reported that a substrate in a supercooled liquid induced short-range translational ordering, whose structure was determined by the final colloidal crystalline state such as body-centered cubic (bcc), hexagonal close packed (hcp), or fcc [76]. The effect of the curvature of the substrate was also investigated, where the seed particles of size $R \geq 5\sigma$ could promote crystal nucleation because of the decrease in nucleation barrier, where σ is the spherical diameter of hard colloids [77].

In the conventional heteroepitaxial growth system, the impact of a substrate on nucleation is measured by the change in the interfacial free energy, $\Delta\sigma$, which comprises the interfacial energies between the substrate/solid, $\sigma_{\text{sub-solid}}$, solid/liquid, $\sigma_{\text{solid-liquid}}$, and substrate/liquid, $\sigma_{\text{sub-liquid}}$ [78]. $\Delta\sigma$ is an important parameter to understand and control the nucleation rate and growth mode of the thin film [79–81]. The shape and size of the nuclei are determined by the balance in the three above-mentioned interfacial free energies.

In a hard-sphere system, the interfacial free energy between solid and liquid, $\sigma_{\text{solid-liquid}}$, for 3D crystals was obtained by computational methods [82]. Yet, the significance of the substrate on the crystallization of 2D colloids was not taken into account. For instance, the monolayer 2D nucleation on a substrate is driven by an applied electric field, where the nucleation behavior is well-explained by CNT but the contribution of the interface energy was not considered [70]. Savage et al. reported that 2D nucleation on a cover glass can proceed through multiple distinct steps (non-CNT model) in the depletion attraction system [83]. The detailed 2D nucleation process on the terrace of colloidal crystals of an attractive system has recently been reported by Nozawa et al. [84], who also did not consider $\Delta\sigma$ because of the 2D islands nucleated on the same material.

These colloidal crystals formed on a foreign substance such as cover glass in the above study; however, the effect of the substrate (interfacial free energy change, $\Delta\sigma$) was neither taken into consideration nor evaluated in these studies. The effect of substrates on colloidal nucleation is yet to be clarified.

1.5 Outline of the thesis

To gain a better understanding of the nucleation process, this thesis focuses on the mechanism of the heterogeneous nucleation of colloidal crystals on substrates by taking the interfacial free energy change ($\Delta\sigma$) into account. The effect of $\Delta\sigma$ on the heterogeneous nucleation of colloidal crystals and the origin of $\Delta\sigma$ were determined by measuring the interaction between colloidal particles and the substrate.

This thesis contains five chapters, which are outlined as follows:

In chapter 1, the background and objective of the thesis are presented.

In chapter 2, the principles and method of colloidal crystallization are introduced. The depletion attraction, employed in the experiment, and the experimental condition are described.

In chapter 3, the *in situ* observation of heterogeneous nucleation of 2D colloidal crystals using cover glass as a substrate is presented. Two types of nucleation processes are found: the conventional 2D nucleation process and the quasi-2D nucleation process. The reason why $\Delta\sigma$ should be accounted for is discussed.

In chapter 4, the nucleation of colloidal crystals on three different substrates--uncoated, Pt-coated, and Au-coated, is examined. The effect of substrate on the nucleation rate is discussed, and the relation between $\Delta\sigma$ and the substrate−particle interactions is evaluated.

In chapter 5, the results of the thesis are summarized.

References

[1] D. Kashchiev. Nucleation-Basic Theory with Applications. Butterworth Heinemann: Boston, **2000**.

[2] M. Sleutel, J. Lutsko, A. E. S. Van Driessche1, M. A. Duran-Olivencia and D. Maes. Observing Classical Nucleation Theory at Work by Monitoring Phase Transitions with Molecular Precision. *Nature Comm.* **2014**, 5, 5598, 1–8.

[3] C. Tape, S. Holtkamp, V. Silwal, et al.. Earthquake Nucleation and Fault Slip Complexity in the Lower Crust of Central Alaska. *Nature Geoscience* **2018**, 11, 536–541.

[4] W. L. Ellsworth and G. C. Beroza. Seismic Evidence for an Earthquake Nucleation Phase. *Science* **1995**, 268, 851–855.

[5] J. Russo and H. Tanaka. The Microscopic Pathway to Crystallization in Supercooled Liquids. *Scientific Reports* **2012**, 505, 1–8.

[6] J. Russo and H. Tanaka. Non-classical Pathways of Crystallization in Colloidal Systems. *MRS Bulletin* **2016**, 41(5), 369–374.

[7] V. J. Anderson, H. N. W. Lekkerkerker. Insights into Phase Transition Kinetics from Colloid Science. *Nature* **2002**, 416, 811–815.

[8] A. Yethiraj, A. van Blaaderen. A Colloidal Model System with an Interaction Tunable from Hard Sphere to Soft and Dipolar. *Nature* **2003**, 421, 513–517.

[9] M. Volmer and A. Weber. Nuclei Formation in Supersaturated States. *Phys. Chem.* **1926**, 119, 277−301.

[10] R. Becker, W. Döring. Kinetic Treatment of Germ Formation in Supersaturated Vapour. *Ann. Phys.* **1935**, 24 (719), 752.

[11] J. Frenkel. A General Theory of Heterophase Fluctuations and Pretransition Phenomena *J. Chem. Phys.* **1939**, 7 (7), 538−547.

[12] X. Y. Liu, Heterogeneous Nucleation or Homogeneous Nucleation? *J. Chem.*

Phys. **2000**. 112, 22 (8), 9949–9955.

[13] V. M. Fokin and E. D. Zanotto. Crystal Nucleation in Silicate Glasses: The Temperature and Size Dependence of Crystal/Liquid Surface Energy. *J. Non-Cryst. Solids* **2000**, 265, 105–112.

[14] A. Laaksonen and I. Napari. Breakdown of the Capillarity Approximation in Binary Nucleation: Density Functional Study. *J. Phys. Chem. B.* **2001**, 105, 11678–11682.

[15] M. A. Sharaf, R. A. Dobbins. A Comparison of Measured Nucleation Rates with the Predictions of Several Theories of Homogeneous Nucleation. *J. Chem. Phys.* **1982**, 77, 1517–1526.

[16] J. W. Gibbs. On the equilibrium of heterogeneous substances. *Trans. Connect. Acad. Sci.* **1876**, 3, 108–248.

[17] J. W. Gibbs. On the equilibrium of heterogeneous substances. *Trans. Connect. Acad. Sci.* **1878**, 16, 343–524.

[18] R. L. Burwell JR. Manual of Symbols and Terminology for Physicochemical Quantities and Units–Appendix II: Definitions, Terminology and Symbols in Colloid and Surface Chemistry. *Pure Appl. Chem.* **1972**, 31, 7551.

[19] P. Pieranski. Colloidal crystals. *Contemporary Physics* **1983**, 24: 25–73.

[20] A. Imhof. Three-Dimensional Photonic Crystals Made from Colloids. In *Nanoscale Materials* Springer, Boston, MA. **2004**, pp423-454.

[21] W. M. Stanley. Isolation of a Crystalline Protein Possessing the Properties of Tobacco-Mosaic Virus. *Science* **1935**, 81, 2113, 644–645.

[22] J. D. Bernal and I. Fankuchen. X-Ray and Crystallographic Studies of Plant Virus Preparations. *The Journal of General Physiology* **1941**.111–146.

[23] R. C. Williams and K. M. Smith. A Crystallizable Insect Virus. *Nature* **1957**, 179(4551), 119.

[24] J. V. Sanders. Colour of Precious Opal. *Nature* **1964**, 204, 1151–1153.

[25] P. J. Darragh, A. J. Gaskin and J. V. Sanders. Opals. *Scient. Am.* **1976** 234, 4, 84.

[26] D. H. Everett. Basic Principles of Colloid Science. *The Royal Society of Chemistry*, London, **1988**.

[27] A. P. Philipse. *Particulate colloids: Aspects of preparation and characterization*. In J. Lycklema, editor, Fundamentals of Interface and Colloid Science, volume IV. Academic Press, London, **2005**.

[28] C. Lopez. Materials Aspects of Photonic Crystals. *Adv. Mater.* **2003**, 15(20), 1679–1704.

[29] Y. Wang, C. Wei, H. Cong, Q. Yang, Y. Wu, B. Su, Y. Zhao, J. Wang, and L. Jiang, Hybrid Top-Down/Bottom-Up Strategy Using Superwettability for the Fabrication of Patterned Colloidal Assembly. *ACS Appl. Mater. Interfaces* **2016**, 8, 4985−4993.

[30] J. Ruan, C. Chen, J. Shen, X. Zhao, S. Qian, and Z. Zhu. A Gelated Colloidal Crystal Attached Lens for Noninvasive Continuous Monitoring of Tear Glucose. Polymers **2017**, 9, 125−137.

[31] J. H. Holtz, J. S. W. Holtz, C. H. Munro, S. A. Asher. Intelligent Polymerized Crystalline Colloidal Arrays: Novel Chemical Sensor Materials. *Anal. Chem.* **1998**, *70 (4)*, 780−791.

[32] H. W. Deckman, J. H. Dunsmuir. Natural Lithography. *Appl. Phys. Lett.* **1982**, 41, 377−379.

[33] H. W. Deckman, J. H. Dunsmuir. Applications of Surface Textures Produced with Natural Lithography. *J. Vac. Sci. Technol. B* **1983**, 1(4), 1109−1112.

[34] J. C. Hulteen, R. P. Van Duyne. Nanosphere Lithography: A Materials General Fabrication Process for Periodic Particle Array Surfaces. *J. Vac. Sci. Technol.*

A **1995**, 13(3), 1553−1558.

[35] C. L. Haynes, R. P. Van Duyne. Nanosphere Lithography: A Versatile Nanofabrication Tool for Studies of Size-Dependent Nanoparticle Optics. *J. Phys. Chem. B* **2001**, 105, 5599−5611.

[36] O. D. Velev, E. W. Kaler, Structured Porous Materials via Colloidal Crystal Templating: From Inorganic Oxides to Metals. *Adv. Mater.* **2000**, 12, No.7, 531–534.

[37] H. Arandiyan, H. Dai, K. Ji, H. Sun, J. Li. Pt Nanoparticles Embedded in Colloidal Crystal Template Derived 3D Ordered Macroporous $Ce_{0.6}Zr_{0.3}Y_{0.1}O_2$: Highly Efficient Catalysts for Methane Combustion. *ACS Catal.* **2015**, *5*, 1781−1793.

[38] Y. Li, X. S. Fang, N. Koshizaki, T. Sasaki, L. Li, S. Y. Gao, et al. Periodic TiO_2 Nanorod Arrays with Hexagonal Nonclose-Packed Arrangements: Excellent Field Emitters by Parameter Optimization. *Adv. Funct. Mater.* **2009**, *19*, 2467−2473.

[39] J. R. Jeong, S. Kim, S. H. Kim, et al. Fabrication of Hexagonal Lattice Co/Pd Multilayer Nanodot Arrays Using Colloidal Lithography. *Small* **2007**, *3*, 1529−1533.

[40] Z. M. Chen, T. Gang, X. Yan, X. Li, et al. Ordered Silica Microspheres Unsymmetrically Coated with Ag Nanoparticles, and Ag-Nanoparticle-Doped Polymer Voids Fabricated by Microcontact Printing and Chemical Reduction. *Adv. Mater.* **2006**, *18*, 924−929.

[41] V. J. Anderson, H. N. W. Lekkerkerker. Insights into Phase Transition Kinetics from Colloids Science. *Nature* **2002**, 416, 811−815.

[42] T. Palberg. Crystallization Kinetics of Colloidal Model Suspensions: Recent Achievements and New Perspectives. *J. Phys.: Condens. Matter* **2014**, *26*,

333101.

[43] W. Poon. Colloids as big atoms. *Science,* **2004**, *304*, 830–831.

[44] A. Vrij, R. Tuinier. Structure of Concentrated Colloidal Dispersions. In J. Lyklema, editor, Fundamentals of Interface and Colloid Science, volume IV, pages 5.1−5.103. Elsevier, Amsterdam, **2005**.

[45] T. Sugimoto, editor. Fine particles: Synthesis, Characterization, and Mechanisms of Growth, *volume 92 of Surfactant science series*. Dekker, New York, **2000**.

[46] E. R. Weeks, J. C. Crocker, A. C. Levitt, et al. Three-Dimensional Direct Space Imaging of Structural Relaxation Near the Colloidal Glass Transition. *Science* **2000**, *287*, 627−631.

[47] Z. Wang, F. Wang, Y. Peng, Z. Zheng, Y. L. Han. Imaging the Homogeneous Nucleation during the Melting of Superheated Colloidal Crystals. *Science* **2012**, *338*, 87−90.

[48] R. Ganapathy, M. R. Buckley, S. J. Gerbode, I. Cohen. Direct Measurements of Island Growth and Step-Edge Barriers in Colloidal Epitaxy. *Science*, **2010**, *327*, 445–448.

[49] K. F. Kelton, A. L. Greer. Nucleation in Condensed Matter -Applications in Materials and Biology. Elsevier: Amsterdam, **2010**.

[50] M. A. Sharaf, R. A. Dobbins. A Comparison of Measured Nucleation Rates with the Predictions of Several Theories of Homogeneous Nucleation. *J. Chem. Phys.* **1982**, 77, 1517–1526.

[51] R. Strey, P. E. Wagner, T. Schmeling. Homogeneous Nucleation Rates for n-Alcohol Vapors Measured in a Two-Piston Expansion Chamber. *J. Chem. Phys.* **1986**, 84, 2325–2335.

[52] A. Laaksonen, R. McGraw, H. Vehkamaki. Liquid-Drop Formalism and Free-

Energy Surfaces in Binary Homogeneous Nucleation Theory. *J. Chem. Phys.* **1999**, 111, 2019–2027.

[53] R. Strey, Y. Viisanen. Measurement of the Molecular Content of Binary Nuclei. Use of the Nucleation Rate Surface for Ethanol-Hexanol. *J. Chem. Phys.* **1993**, 99, 4693–4704.

[54] J. Drenth, C. Haas. Nucleation in Protein Crystallization. *Acta Crystallogr., Sect. D: Biol. Crystallogr.* **1998**, 54, 867–872.

[55] V. M. Fokin, E. D. Zanotto. Crystal Nucleation in Silicate Glasses: The Temperature and Size Dependence of Crystal/Liquid Surface Energy. *J. Non-Cryst. Solids* **2000**, 265, 105–112.

[56] D. W. Oxtoby. Nucleation of First-Order Phase Transitions. *Acc. Chem. Res.* **1998**, 31, 91–97.

[57] F. Schuth. Nucleation and Crystallization of Solids from Solution. Curr. Opin. *Solid State Mater. Sci.* **2001**, 5, 389–395.

[58] M. H. Nielsen, S. Aloni, J. J. D. Yoreo. In situ TEM imaging of CaCO3 nucleation reveals coexistence of direct and indirect pathways. *Science* **2014**, 345, 1158–1162.

[59] M. Sleute, J. Lutsko, A. E. Van Driessche, M. A. Durán-Olivencia and D. Maes. Observing classical nucleation theory at work by monitoring phase transitions with molecular precision. *Nature Communications* **2014**, 5, 5598, 1–8.

[60] G. C. Sosso, J. Chen, S. J. Cox. M. Fitzner, P. Pedevilla, A. Zen and A. Michaelides. Crystal Nucleation in Liquids: Open Questions and Future Challenges in Molecular Dynamics Simulations. *Chem. Rev.* **2016**, 116, 7078–7116

[61] E. Auyeung, T. I. N. G. Li, A. J. Senesi, A. L. Schmucker, B. C. Pals, M. O.

de la Cruz and C. A. Mirkin. DNA-mediated Nanoparticle Crystallization into Wulff Polyhedral. *Nature* **2014**, 505, 73–77.

[62] F. Lu, K. G. Yager, Y. G. Zhang, H. L. Xin and O. Gang. Superlattices Assembled through Shape-induced Directional Binding. *Nat. Comm.* **2015**. 6:6912, 1–10.

[63] P. R. ten Wolde and D. Frenkel. Enhancement of Protein Crystal Nucleation by Critical Density Fluctuations. *Science* **1997**, 277, 1975–1978.

[64] T. H. Zhang and X. Y. Liu. Multistep Crystal Nucleation: A Kinetic Study Based on Colloidal Crystallization. *J. Am. Chem. Soc.***2007,** 129, 13520–13526.

[65] Y. Peng, F. Wang, Z. Wang, A. M. Alsayed, Z. Zhang, A. G. Yodh and Y. L. Han. Two-step Nucleation Mechanism in Solid–Solid Phase Transitions. *Nature Materials* **2014**, 14, 101–108.

[66] K. Schaetzel and B. J. Ackerson. Density Fluctuations during Crystallization of Colloids. *Phys. Rev. E* **1993**, 48, 3766–77.

[67] U. Gasser, E. R. Weeks, A. Schofield, P. N. Pusey and D. A. Weitz. Real-space Imaging of Nucleation and Growth in Colloidal Crystallization. *Science* **2001**, 292, 258–62.

[68] B. O'Malley and I. Snook. Crystal Nucleation in the Hard Sphere System. *Phys. Rev. Lett.* **2003**. 90, 085702.

[69] S. Auer, D. Frenkel. LineTension Controls Wall-Induced Crystal Nucleation in Hard-Sphere Colloids. *Phys. Rev. Lett.* **2003**, *9(1)*, 015703-1−4.

[70] K. Q. Zhang, X. Y. Liu. In Situ Observation of Colloidal Monolayer Nucleation Driven by An Alternating Electric Field, *Nature* **2004**, *429*, 739−743.

[71] C. M. Wayman, T. P. Darby. Nucleation and Growth of Gold Films on Graphite. *J. of Cryst. Growth* **1975**, *28*, 53–67.

[72] R. Hull, A. Fischer-Colbrie, S. J. Rosner, S. M. Koch and J. S. Harris Jr. Effect of Substrate Surface Structure on Nucleation of GaAs on Si (100). *Appl. Phys. Lett.* **1987**, 51 (21), 23, 1723–1725.

[73] A. V. Blaaderen, R. Ruel and P. Wiltzius. Template-directed colloidal crystallization. *Nature* **1997**, *385*, 321–324.

[74] K. Sandomirski, E. Allahyarov, H. Löwen and S. U. Egelhaaf. Heterogeneous Crystallization of Hard-sphere Colloids near a Wall. *Soft Matter* **2011**, *7*, 8050–8055.

[75] P. Jiang, J. F. Bertone, K. S. Hwang and V. L. Colvin. Single-crystal Colloidal Multilayers of Controlled Thickness. *Chem. Mater.* **1999**, 11, 2132−2140.

[76] S. Arai, H. Tanaka. Surface-assisted Single-crystal Formation of Charged Colloids. *Nat. Phys.*, **2017**, 13, 503−509.

[77] A. Cacciuto, S. Auer and D. Frenkel. Onset of Heterogeneous Crystal Nucleation in Colloidal Suspensions. *Nature* **2004**, 428, 404−406.

[78] V. Talanquer, D. W. and Oxtoby. Nucleation on a Solid Substrate: A Density Functional Approach, *J. Chem. Phys.* **1996**, 104 (4), 22, 1483−1492.

[79] W. R. Tyson. Surface Free Energies of Solid Metals Estimation from Liquid Surface Tension Measurements. *Surf. Sci.*, **1977**, 62, 267−276.

[80] H. Shu, D. Cao, P. Liang, X. Wang, X. Chen and W. Lu. Two-dimensional Silicene Nucleation on a Ag (111) Surface: Structural Evolution and the Role of Surface Diffusion. *Phys. Chem. Chem. Phys.* **2014**, 16, 304−310.

[81] W. Xu, Z. Lan, B. L. Peng, R. F. Wen and X. H. Ma. Effect of Surface Free Energies on the Heterogeneous Nucleation of Water Droplet: A Molecular Dynamics Simulation Approach. *J. Chem. Phys.* **2015**, 142, 054701-1−12.

[82] R. L. Davidchack. Hard Spheres Revisited: Accurate Calculation of the Solid-Liquid Interfacial Free Energy. *J. Chem. Phys.* **2010**, 133, 234701-1.

[83] J. R. Savage and A. D. Dinsmore. Experimental Evidence for Two-Step Nucleation in Colloidal Crystallization. *Phys. Rev. Lett.* **2009**, 102, 1983021–1983024.

[84] J. Nozawa, S. Uda, S. X. Guo, S. M. Hu, A. Toyotama, J. Yamanaka, J. Okada and H. Koizumi. Two-Dimensional Nucleation on the Terrace of Colloidal Crystals with Added Polymers. *Langmuir* **2017,** 33(13), 3262–3269.

Chapter 2 Crystallization of colloidal crystals

There are many methods for obtaining colloidal crystals, of which the depletion attraction method is adopted in this study. This chapter discusses the principle of each method. After which, the experimental procedures used are introduced.

2.1 Principles of colloidal crystallization

In this study, the nucleation of 2D colloidal crystals was investigated. There are various methods for the fabrication of 2D colloidal crystals, including solvent evaporation [1], spin coating [2], electric field-induced flow [3], and depletion attraction [4]. These methods are classified as hard sphere, repulsive, and attractive systems in terms of particle interaction.

In the hard sphere system, the pair interaction, U, between particles of diameter a is approximated as [5]

$$U(d)=\infty \quad d < a,$$
$$=0 \quad d \geq a, \tag{2.1}$$

where d is the center-to-center distance of the particles, as plotted in Figure 2.1a. Since no potential energy exists between the hard spheres, the phase behavior is dependent on the volume fraction, Φ, as illustrated in Figure 2.2. Colloidal crystallization occurs when the volume fraction attains a value of 0.49 [6]. The fluid and crystal coexist between the freezing point, Φ_F, and the melting point, Φ_M. The crystal is stable when Φ exceeds the melting point, Φ_M, 0.545. Glass transition is observed at a volume fraction of 0.58 [6, 7]. Hexagonally close-packed crystals form at the maximum volume fraction, Φ_{CP}, 0.74, while in random close-packed structures, Φ_{CP} reduces to 0.64.

The interaction between particles in the repulsive system is shown in Figure 2.1b. Repulsive forces between particles can be tuned by the ionic strength of the solution and pH or surface charge density of particles. Different repulsive interactions such as dipolar interactions, Coulomb interaction, and steric stabilization are shown in Figure 2.3 [8]. The interaction between particles in the attractive system is presented in Figure 2.1c; attractive interactions work between particles, such as immersion capillary forces, Coulomb attraction, van der Waals (vdW) attraction, and the depletion attraction by the addition of polymers, as shown in Figure 2.4 [8]. The phase diagram of the attractive system is presented in Figure 2.5 [9], which corresponds to the hard sphere system without polymer, as shown in Figure 2.2.

The theory of Derjaguin, Landau, Verwey and Overbeek (DLVO) was employed to explain particle interaction in stabilized colloidal dispersions [10, 11]. The van der Waals (vdW) attractions and electrostatic double-layer repulsion compose interparticle interaction in the DLVO theory, as expressed in Eq. 2.2.

$$F = F_{vdW} + F_{dl} \tag{2.2}$$

where F_{vdW} is the vdW attraction and F_{dl} is the double-layer force. The total DLVO interaction potential is shown in Figure 2.1d, where the potential of three different cases is summarized. The electrostatic double-layer repulsion dominates at a low ionic strength in (I), causing the colloidal particles to be dispersed. There is a secondary minimum potential at the intermediate ionic strength in (II), leading to a negligible barrier. The attraction is over the double layer repulsion between the colloidal particles at high ionic strengths in (III). The interaction between particles is tuned as a result of the competition between vdW attraction and double-layer repulsion.

The growth mode of colloidal crystals depends on particle interaction. In

the hard-sphere and repulsive system, the densities of the solid and liquid are similar, and thus, an ambiguous interface is formed [12]. The growth mode is similar to that of the melt growth. A smooth interface is developed in the attractive system for a large density difference between the liquid and solid, where the growth mode is analogous to that of the solution or vapor growth. Two-dimensional nucleation is clearly observed in the attractive system [13], which meets the requirement for the study on heterogeneous nucleation on a substrate. Therefore, the attractive system is utilized in this study.

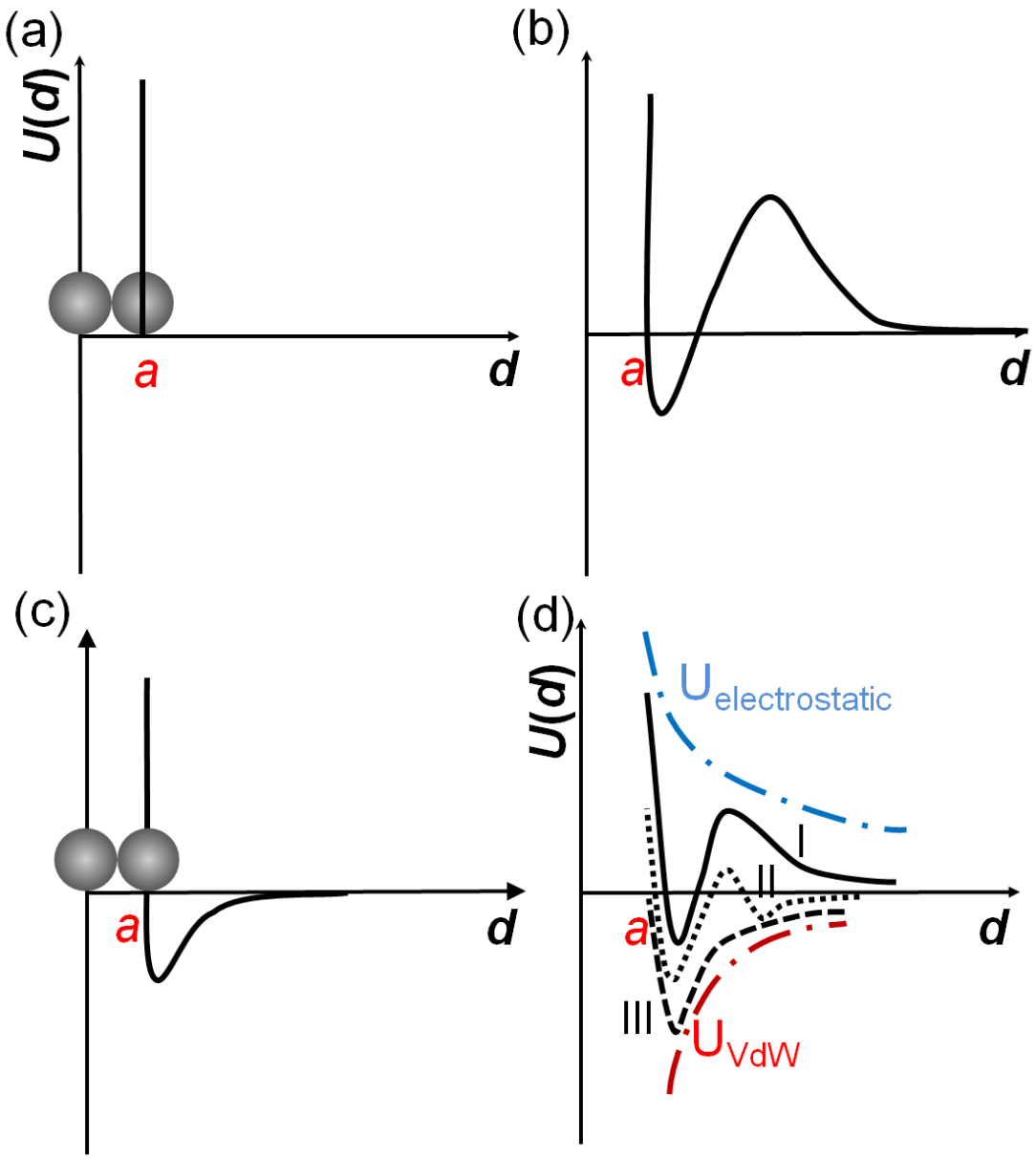

Figure 2.1 Pair interaction between colloidal particles, where *a* is the diameter of a particle: (a) Hard sphere interaction, (b) repulsive interaction, (c) attractive interaction. (d) Schematic representation of DVLO interaction. Curves (I), (II), and (III) correspond to the three distinct conditions upon which increasing the concentration of electrolytes depends.

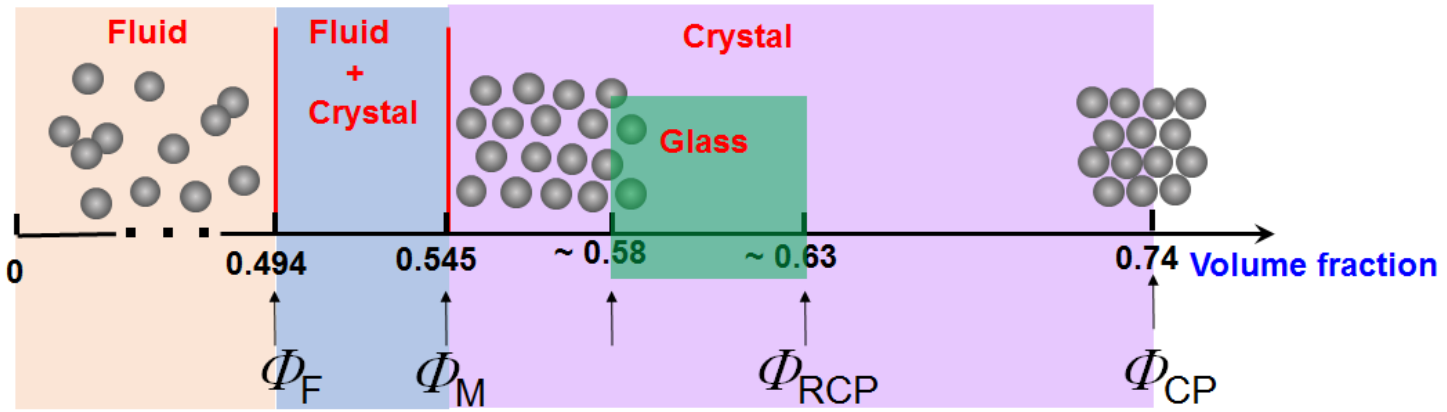

Figure 2.2 Phase behavior of hard-sphere particles based on the volume fraction, where Φ, Φ_F, Φ_M, Φ_{RCP}, and Φ_{CP} represent the volume fractions for freezing, melting, random close-packed, and close-packed points, respectively.

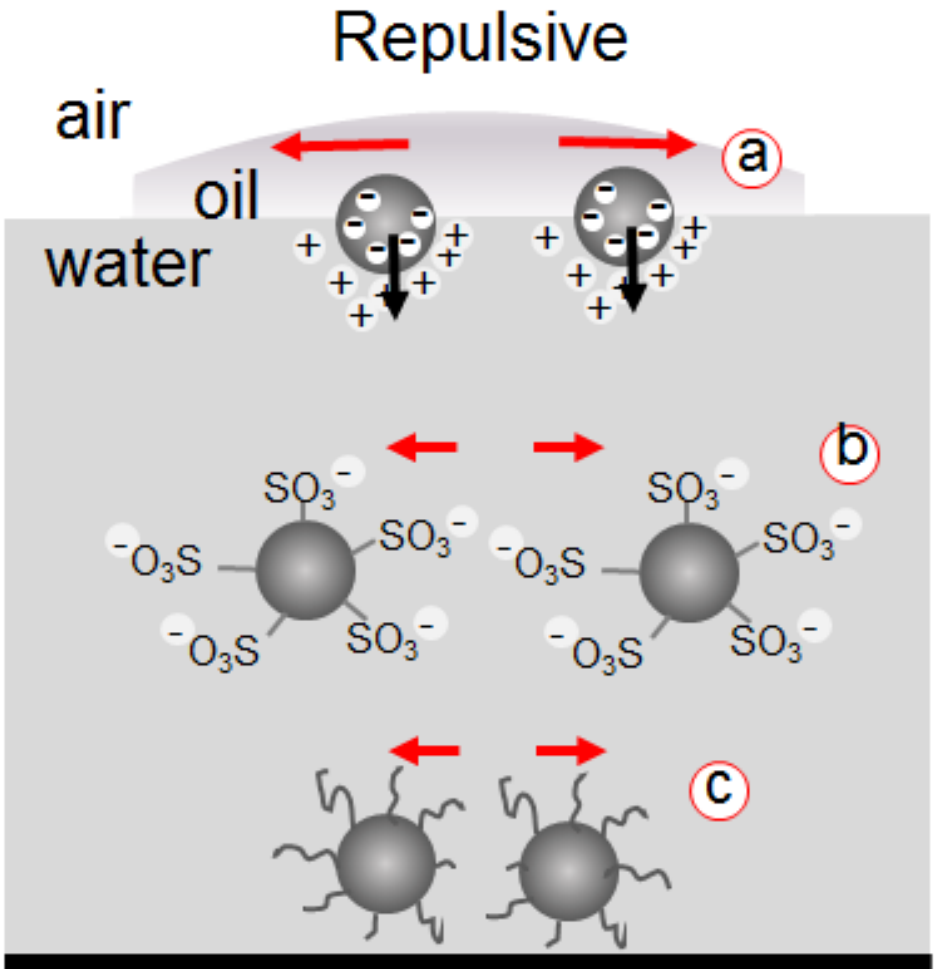

Figure 2.3 Repulsive interparticle interactions: (a) dipolar repulsion by partial ionic dissociation at the interfaces, (b) Coulomb repulsion, (c) steric repulsion. Readapted with permission from [8]. Copyright (2015) American Chemical Society.

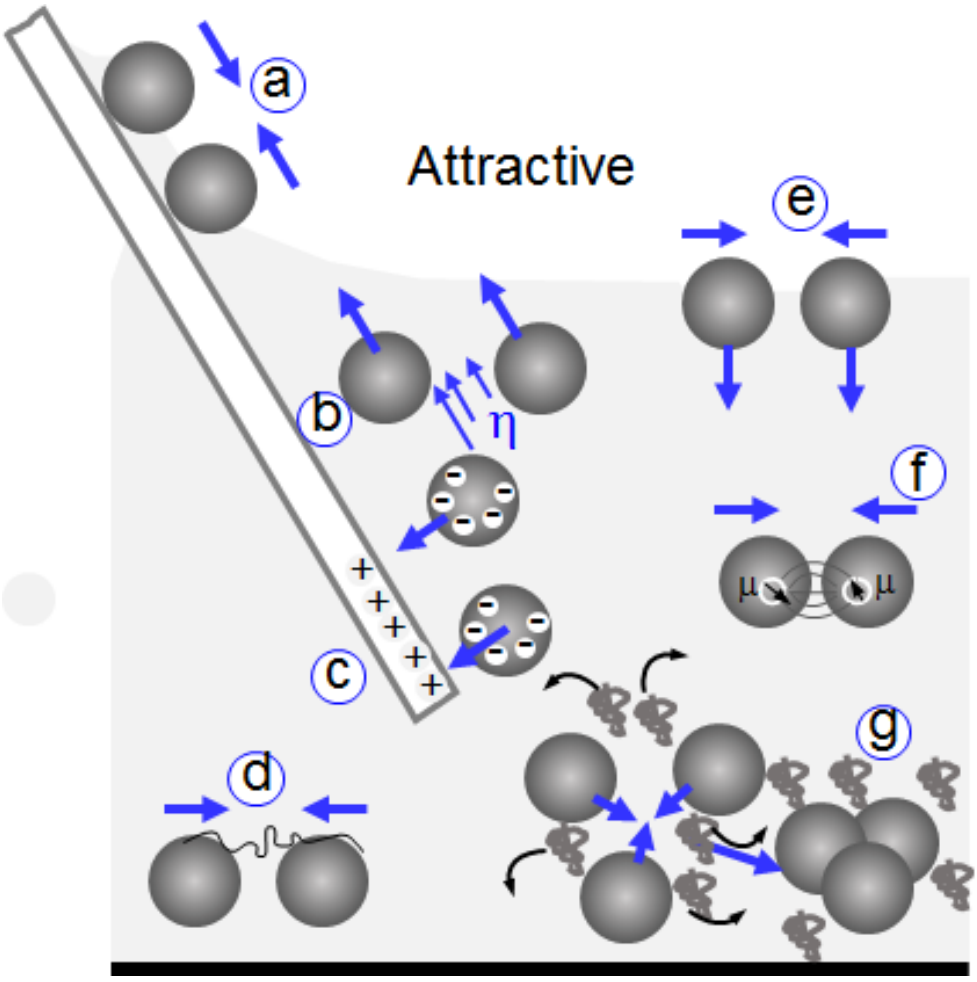

Figure 2.4 Attractive interactions: (a) Immersion capillary forces, (b) hydrodynamic coupling/drag forces, (c) Coulomb attraction to oppositely charged surfaces, (d) bridging attraction/flocculation, (e) flotation capillary forces, (f) vdW attraction, and (g) depletion attraction. Readapted with permission from [8]. Copyright (2015) American Chemical Society.

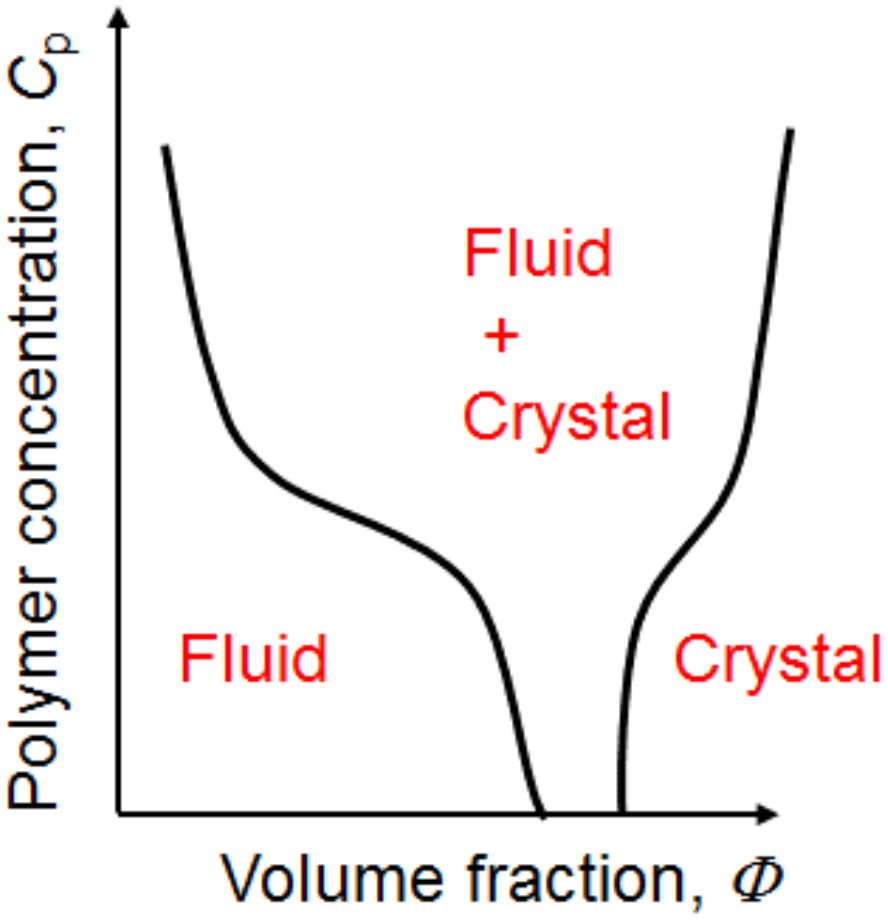

Figure 2.5 Phase diagram of the attractive system. At polymer concentration, C_p= 0 corresponds to Figure 2.2.

2.2 Attractive system-depletion attraction

As described in the previous section, the attractive system was employed in this study. The depletion attraction interaction was employed for the crystallization process. This method is one of the most convenient methods because it works on any type of particle without the need for modifying the particle surface. The depletion attractive interaction has been widely applied to model phase transitions such as superheating [14].

The principle of depletion attraction is shown in Figure 2.6 [15]. For charged colloidal particles, repulsive interaction works between particles in the water solution, as illustrated in Figure 2.6a. When a polymer is added to the solution, the depletion layers are formed around the particles (indicated by the dashed circles in Figure 2.6b) because the surrounding of the colloidal particle is unavailable for the center of the polymer to occupy. This layer indicates the excluded volumes of the depletant. When the particles are close to each other, the depletion layers overlap. The polymer cannot enter the overlapped area between the particles whose sizes are smaller than that of the polymer in the solution. Such overlapped area is referred to as the depletion zone. The concentration of the polymer between the depletion zone and other regions is different, as it generates osmotic pressure, Δp. The difference in the osmotic pressure leads to a depletion attraction between particles.

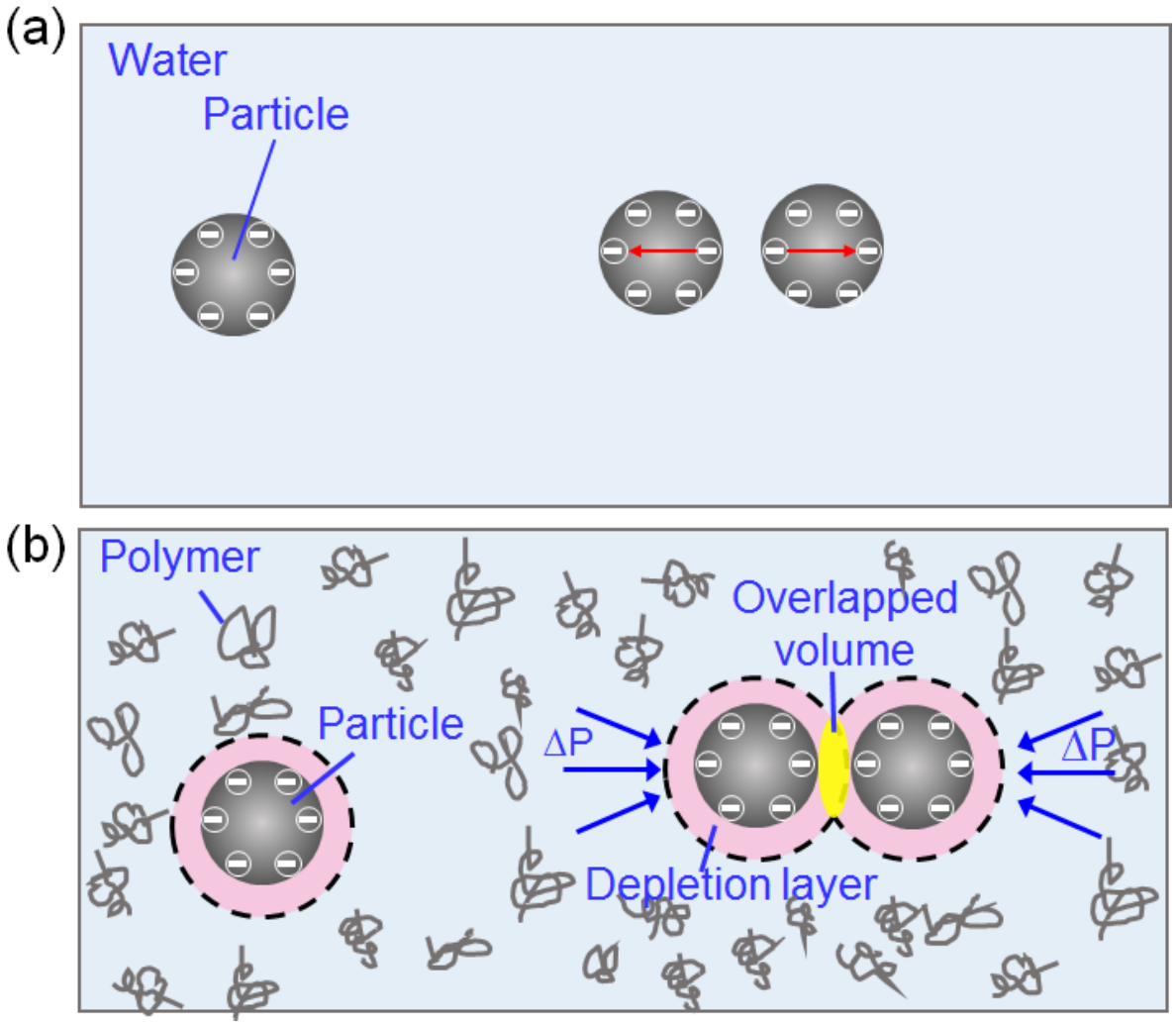

Figure 2.6 Illustration of depletion attraction. (a) Colloidal particles in water, (b) particles after the addition of polymer.

2.3 Experimental

The colloidal particles employed in the experiments were green fluorescent 500 nm monodispersed polystyrene spheres (PS) (Thermo Fisher Scientific). The zeta potential of the PS particles was measured as −47.1 ± 5.9 mV. A negatively charged sodium polyacrylate polymer (polymerization degree of 30000–40000) was dispersed into the PS suspensions as the depletant to generate an attractive force between the particles and the substrate as well as between the particles. The concentration of sodium polyacrylate was 0.15 g/L for all experiments. The volume fractions (Φ) of initial colloidal suspensions ranged from 0.05 to 1%. Three different substrates, uncoated, Au-coated and Pt-coated cover glasses, were used (Figure 2.7 (a)). A cover glass with a thickness of 0.12–0.17 mm was employed after cleaning with deionized water. Au or Pt thin layers (~12 nm in thickness) were coated on the cover glass by the sputter coating technique (SC-701AT, Sanyu Electron Inc.).

The solution was sealed in a growth cell composed of a silicone sheet as a spacer (2 mm thickness) and cover glass as a substrate as shown in Figure 2.7 (b). All of the experiments were performed under ambient conditions (*ca*. 25 °C). Crystallization occurred on the substrates at the bottom of the cell, and was observed by inversed optical microscopy. An oil immersion lens (magnification = 100 and N.A. = 1.3) was utilized to achieve single particle resolution of 500 nm particles.

Colloidal crystallization is caused by a depletion attraction. [13, 15] The interparticle interactions can be tuned by the concentration of a polymer. The attractive potential of particles is calculated in terms of depletion potentials and van der Waals (VDW) as follows. The strength of the depletion attractive potential, $U_{AO}(d)$, was derived by Asakura-Oosawa [16] and Vrij [17] as:

$$U_{AO}(d) = -n_b k_B T V_{OV}(d) \quad (a \le d \le 2R_d) \tag{2.3}$$

$$=0 \qquad (d > 2R_d) \tag{2.4}$$

where n_b is the polymer number density, R_d is the depletion radius which is obtained as the sum of the particle radius (a/2) and the radius of gyration of the polymer in water (R_g), $V_{OV}(d)$ is the overlap volume of spheres that have radii of R_d, d is the center-to-center distance of the particles, k_B is the Boltzmann constant and T is the absolute temperature. $V_{OV}(d)$ is derived as:

$$V_{OV}(d) = \frac{4\pi}{3} R_d^3 \left[1 - \frac{3}{4}\frac{d}{R_d} + \frac{1}{16}\left(\frac{d}{R_d}\right)^3 \right] \tag{2.5}$$

R_g was determined by dynamic light scattering (DLS) to be 100 nm. The value of n_b is obtained [5]

$$\frac{n_b}{n_b^*} = \frac{\varphi}{\varphi^*} \tag{2.6}$$

where n_b^* is the polymer number density at which the polymer coils overlap, φ is weight fraction of the polymer, and φ^* is weight fraction of the polymer where the chains start to overlap.

The concentration of polymer by weight, φ, is calculated to be 0.14×10^{-3} wt%. The value of φ^* is calculated by $\varphi^* = 10^3 M_w n_b^* / N_A$, where M_w is weight average molecular weight, which is obtained from the degree of polymerization (30000-40000) to be $M_w = 94\times3.5\times10^4 = 3.3\times10^6$, in which 35000 was used as an average

value of the degree of polymerization.

Since $n_b^* = \frac{3}{4\pi R_g^3}$, equation 2.6 is transformed into

$$n_b = \frac{\varphi}{\varphi^*} \times n_b^* = \frac{\varphi N_A}{10^3 M_W}.$$

The n_b is calculated to be 0.26×10^{11}/g. The values of each parameter are substituted into equation 1 to obtain the potential of depletion attraction as a function of center-to-center distance, which is shown as blue line in Figure 2.8.

The VDW potential between two particles is given by

$$U_{VDW}(d) = -\frac{A_H}{6}\left(\frac{a^2}{2}\left(\frac{1}{d^2-(a)^2}+\frac{1}{d^2}\right)+\ln\frac{d^2-(a)^2}{d^2}\right) \quad (2.7)$$

Where A_H is the Hamaker constant. [18] U_{VDW} and U_{AO}+ U_{VDW} are shown in orange and black line in Figure 2.8, respectively. Crystallization occurs on the cover glass. In the polymer added solution, there are two depletion forces at work, one between particles and substrate and one between the particles themselves. Though the 500 nm particles exhibit strong Brownian motion, the depletion attraction between the particles and the substrate causes the particles to stay on the substrate.

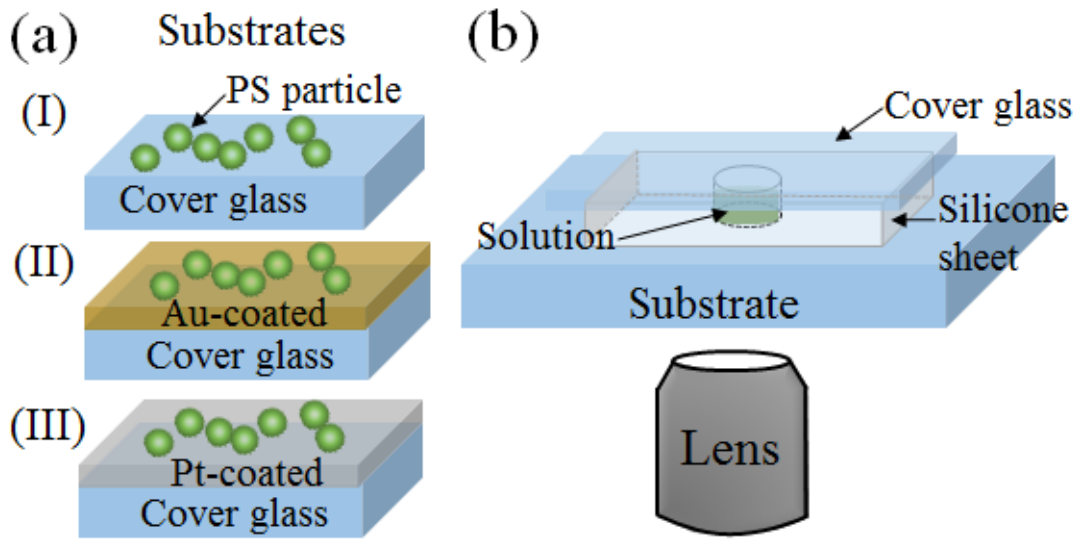

Figure 2.7 (a) Cover glass (I), Au-coated cover glass (II) and Pt-coated cover glass (III) substrates. (b) Schematic illustration of the growth cell for the colloidal crystals.

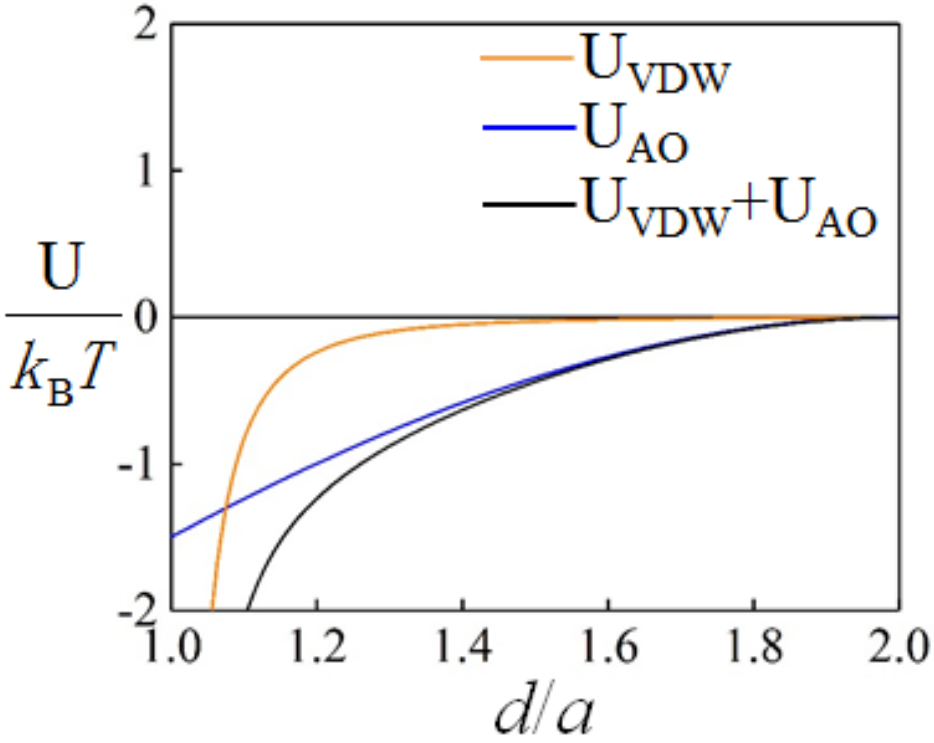

Figure 2.8 Attractive potential between the particles. *d* is the center-to-center distance of the particles, *a* is the diameter of the particles. The interaction potential of van der Waals (VDW), U_{VDW}, and depletion attraction, U_{AO}, are show in blue and orange line, respectively. The sum of them is shown in black line.

The interaction forces between a polystyrene particle and a substrate were measured as a function of the surface separation distance (D) using colloidal probe atomic force microscopy. [19, 20] A schematic illustration of the setup is shown in Figure 2.9. A commercial AFM (SPI3800-SPA400, SII NanoTechnology Inc.) in combination with a homemade closed fluid cell was used for the interaction forces measurement in aqueous solution. The colloidal probe was prepared by attaching a colloidal sphere (polystyrene, 10 μm in diameter) to the end of a cantilever (DNP-S, Bruker Nano Inc.) with UV curable resin (NOA61, Norland Products Inc.). The details of the surface force measurement are described Chapter 4.

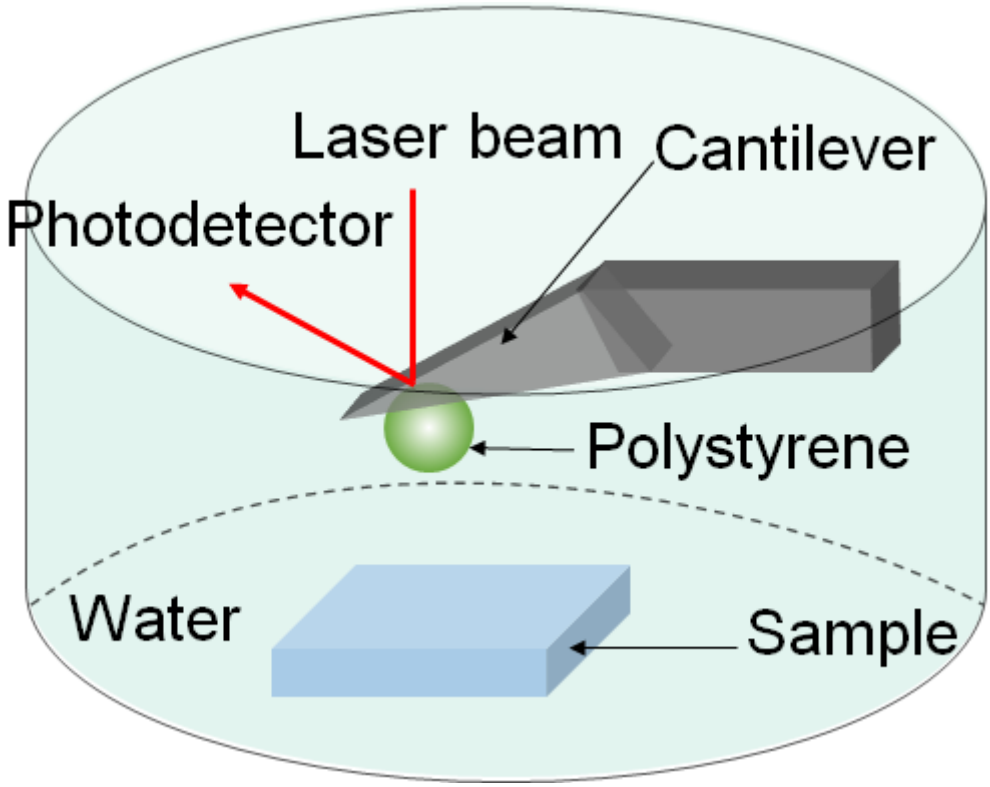

Figure 2.9 Schematic illustration of the colloidal AFM probe for measuring interactions between the polystyrene particle and the substrate.

References

[1] M. H. Kim, S. H. Im, O. O. Park. Rapid Fabrication of Two- and Three-Dimensional Colloidal Crystal Films via Confined Convective Assembly. *Adv. Funct. Mater.* **2005**, 15, 1329−1335.

[2] E. Armstrong, W. Khunsin, M. Osiak, M. Blömker, C. M. Sotomayor Torres, C. O'Dwyer. Ordered 2D Colloidal Photonic Crystals on Gold Substrates by Surfactant-Assisted Fast-Rate Dip Coating. *Small* **2014**, 10, No.10, 1895−1901.

[3] K. Q. Zhang, X. Y. Liu. In Situ Observation of Colloidal Monolayer Nucleation Driven by an Alternating Electric Field. *Nature* **2004**, 429, 739−743.

[4] A. Toyotama, T. Okuzono, J. Yamanaka. Spontaneous formation of eutectic crystal structures in binary and ternary charged colloids due to depletion attraction. *Scientific reports*, **2016**, 6, 23292-1−9.

[5] A. Yethiraj. Tunable colloids: control of colloidal phase transitions with tunable interactions. *Soft Matter*, **2007**, 3, 1099–1115. H. N.W. Lekkerkerker and R. Tuinier. Colloids and the Depletion Interaction. *Springer: Netherlands*, **2011**, chapter 1.

[6] P. N. Pusey, W. van Megen. Phase behavior of concentrated suspensions of nearly hard colloidal spheres. *Nature* **1986**, *320*, 340–342.

[7] L. Cipelletti and L. Ramos. Slow dynamics in glassy soft matter. *J. Phys.: Condens. Matter* **2005**, 17, R253–85.

[8] N. Vogel, M. Retsch, C. Fustin, A. Campo, and U. Jonas. Advances in Colloidal Assembly: The Design of Structure and Hierarchy in Two and Three Dimensions. *Chem. Rev.* **2015**, 115, 6265−6311.

[9] H. N.W. Lekkerkerker and R. Tuinier. Colloids and the Depletion Interaction.

Springer: Netherlands, **2011**, chapter 5.

[10] B. V. Derjaguin, L. Landau. Theory of the stability of strongly charged lyophobic sols and of the adhesion of strongly charged particles in solutions of electrolytes. *Acta Phys Chim USSR* **1941**, *14*, 633–662.

[11] E. J. W. Verwey, J. T. G. Overbeek. *Theory of the stability of lyophobic colloids*. Elsevier, Amsterdam, **1948**.

[12] A. Stefan and F. Daan. Prediction of absolute crystal-nucleation rate in hard-sphere colloids. *Nature* **2001**, 409, 6823, 1020–1023.

[13] J. Nozawa, S. Uda, S. X. Guo, S. M. Hu, A. Toyotama, J. Yamanaka, J. Okada and H. Koizumi. Two-Dimensional Nucleation on the Terrace of Colloidal Crystals with Added Polymers. *Langmuir* **2017,** 33(13), 3262–3269.

[14] Z. Wang, F. Wang, Y. Peng, Z. Zheng, Y. Han. Imaging the Homogeneous Nucleation during the Melting of Superheated Colloidal Crystals. *Science* **2012**, 338, 87−90.

[15] A. S. Karas, J. Glaser, S. C. Glotzer. Using Depletion to Control Colloidal Crystal Assemblies of Hard Cuboctahedra, *Soft Matter* **2016**, *12*, 5199−5204.

[16] S. Asakura, F. Osawa. On Interaction between two Bodies Immersed in a Solution of Macromolecules. *J.Chem. Phys.* **1954**, 22, 1255–1256.

[17] A. Vrij. Polymers at Interfaces and the Interactions in Colloidal Dispersions. *Pure Appl. Chem.***1976**, 48, 471–483.

[18] J. Israelachvili. *Intermolecular and Surface Forces*, 2nd ed., Academic press, London, 2011. Chapter 6.

[19] H. J. Butt. Measuring electrostatic, van der Waals, and hydration forces in electrolyte solutions with an atomic force microscope, *Biophys. J.* **1991**, *60*, 1438−1444.

[20] W. A. Ducker, T. J. Senden, R. M. Pashley. Direct measurement of colloidal

forces using an atomic force microscope, *Nature* **1991**, *353*, 239.

Chapter 3 The heterogeneous nucleation of colloidal crystals on a glass substrate

Based on the principle of depletion attraction described in chapter 2, the heterogeneous nucleation of colloidal crystals on a cover glass substrate was performed in this chapter. The nucleation process of colloidal crystals was investigated by *in situ* observation.

3.1 Two types of nucleation process on the cover glass

After mixing the colloidal suspension and the polymer, 2D nucleation takes place on the glass substrate at the bottom of the cell. First, with particles sinking due to gravity, the particle concentration in the vicinity of the glass substrate increases. As colloidal particles collide with each other, they form clusters. Some clusters shrink and disappear, while others continue to grow in the lateral direction to become nuclei, forming the 1st layer. The secondary layer occurs on the surface of the grown clusters. In the experimental time period, about 5 layers develop by the repetition of similar processes. The concentration of colloidal particles in the solution decreases over time because the particles are consumed for nucleation and growth. As the particle concentration decreases, only growth takes place, because a higher concentration is required for nucleation than for growth. When the particle concentration decreases to a certain value, growth then ceases.

In this nucleation process, we discovered two strategies of nucleation: one occurs with a mono-layer and the other with two layers. In the former case, mono-layer nucleation, the cluster overcomes the critical size with a mono-layer,

which is equivalent to 2D nucleation. In the latter case, quasi-two-dimensional nucleation (q-2D nucleation), the cluster overcomes the critical size by forming a two-layer structure. We call the two-layer structure a quasi-two-dimensional (q-2D) nucleation. Though the nucleus has two layers, it is not categorized as a three-dimensional (3D) nucleus because it does not have a 3D shape. To have a 3D shape, the ratio of the number of particles for each layer should be constant for any nucleus size; however, it is not constant for the q-2D nuclei observed in the present study. We classified this structure as q-2D. The q-2D structure is only observed for nucleation on a glass substrate, not for 2D nucleation on the terrace substrate of colloidal crystals. Therefore, this is characteristic of the nucleation process on a glass substrate, and further detailed observations were then carried out.

3.1.1 Monolayer nucleation

Figure 3.1 shows the mono-layer nucleation process on the glass substrate by *in situ* observations. The images were taken immediately after solution preparation. The experiments were carried out at room temperature (25 ºC). The polymer concentration was 0.15 g/L. Some clusters with a mono-layer, enclosed in dashed white circles, shrink and eventually dissolve, whereas some others, enclosed in dashed red, keep growing. Figure 3.2 shows the same phenomenon on the cover glass under different colloidal concentrations. These suggest that a critical size for the nucleation process exists. In the nucleation process, a cluster overcomes the critical size by forming a mono-layer. We determined the critical size from the largest clusters that are not stable and still tend to dissolve.

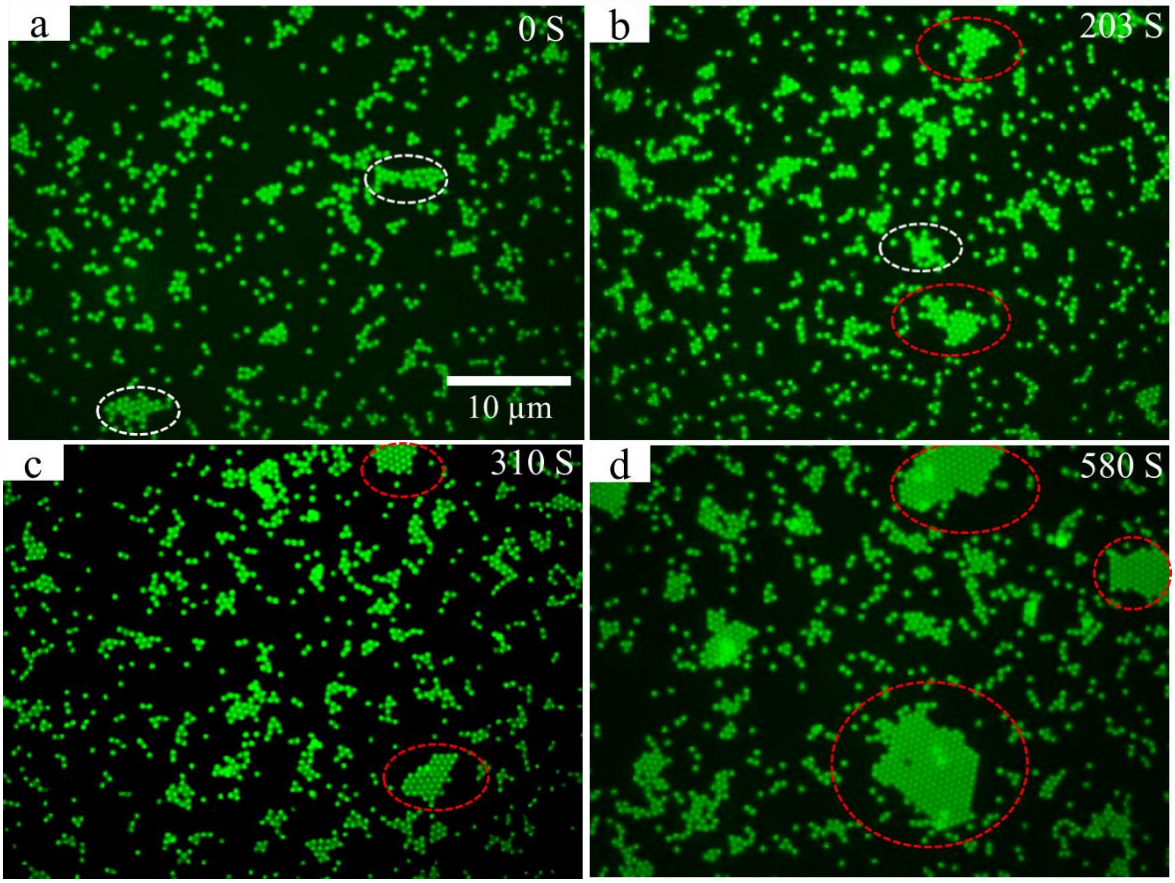

Figure 3.1 Snapshots of the mono-layer nucleation process on the glass substrate. The clusters in dashed white circles disappear as shown in (a) and (b), while clusters in dashed red circles continue to grow as shown in (b), (c), and (d).

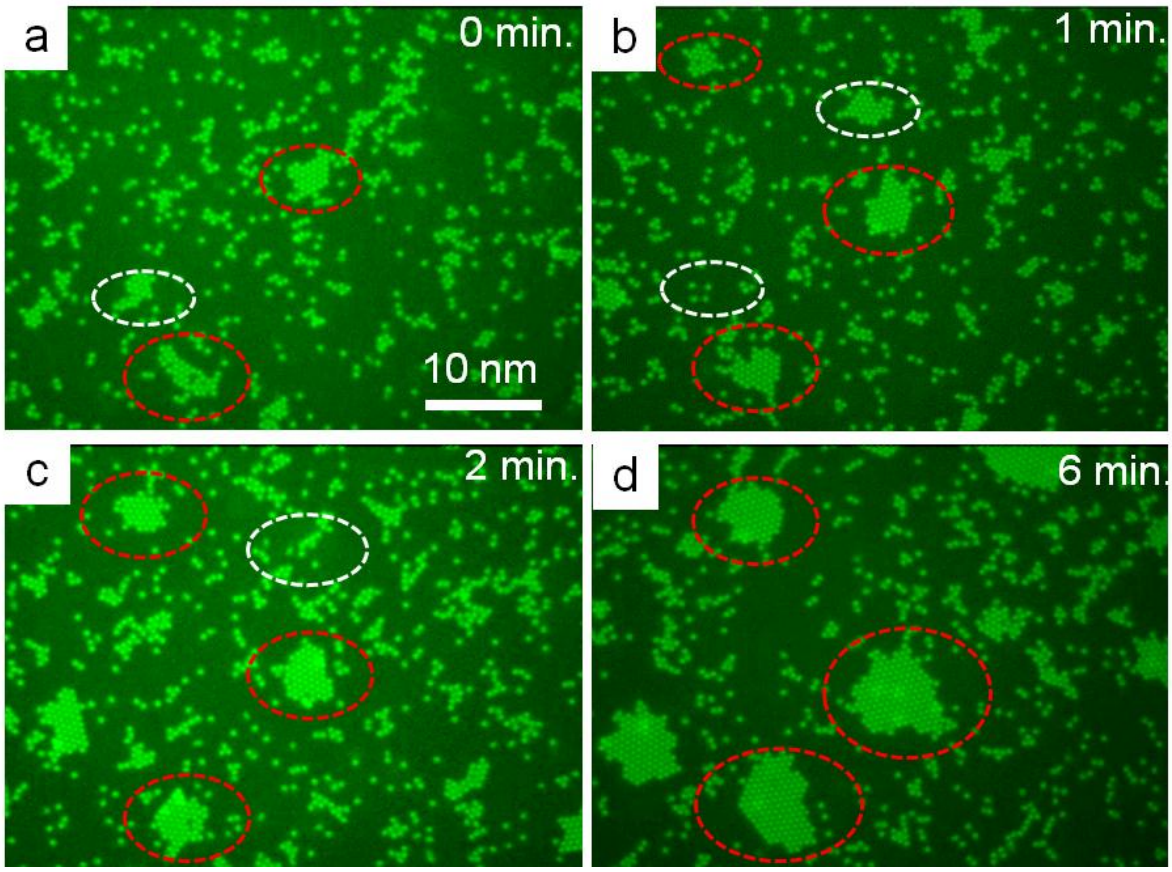

Figure 3.2 Snapshots of the mono-layer nucleation process on the glass substrate. The clusters in dashed white circles disappear as shown in (a), (b) and (c), while clusters in dashed red circles continue to grow as shown in (a), (b), (c), and (d).

3.1.2 Quasi-2D nucleation

We also observed q-2D nuclei formation where the 2nd layer forms on the 1st layer as shown in Figure 3.3. The images were taken several minutes after the solution was added into the growth cell. Two mono-layer embryos that appeared on the glass substrate are enclosed by a dashed white circle (I) and a dashed yellow circle (II) in Figure 3.3 (a). Several seconds later, a 2nd layer appears on the 1st layer in the enclosed dashed yellow embryo as shown in Figure 3. 3 (b), where the inset shows a schematic of the q-2D structure. The embryos continues growing as seen in the dashed yellow circle (c–f). This nucleation process does not correspond to so-called two-step nucleation. Even though formation of the 2nd layer followed formation of the 1st layer, there is no intermediate phase that transforms into the final phase. Both 1st and 2nd layers constitute the building unit of the two-layer structure. On the other hand, the mono-layer structure shrinks and then disappears as seen in the dashed white circle (b–c). Though the number of particles in the q-2D structure is smaller than that of the mono-layer structure in Figure 3.3 (a), the former nucleates whereas the latter disappears. It should be noted that when subcritical embryos of the 2nd layer are growing at the edge, the nucleation process is probably affected by the boundary of the 1st layer because growth of the 2nd layer is inhibited by the boundary. The nucleation rate may be reduced due to this effect. However, we do not have enough data to quantitatively evaluate the effect on the nucleation rate. This will be investigated in future studies. This quasi-2D nucleation phenomenon was observed on the cover glass as well as other substrates, such as the Pt-coated cover glass, as shown in Figure 3.4.

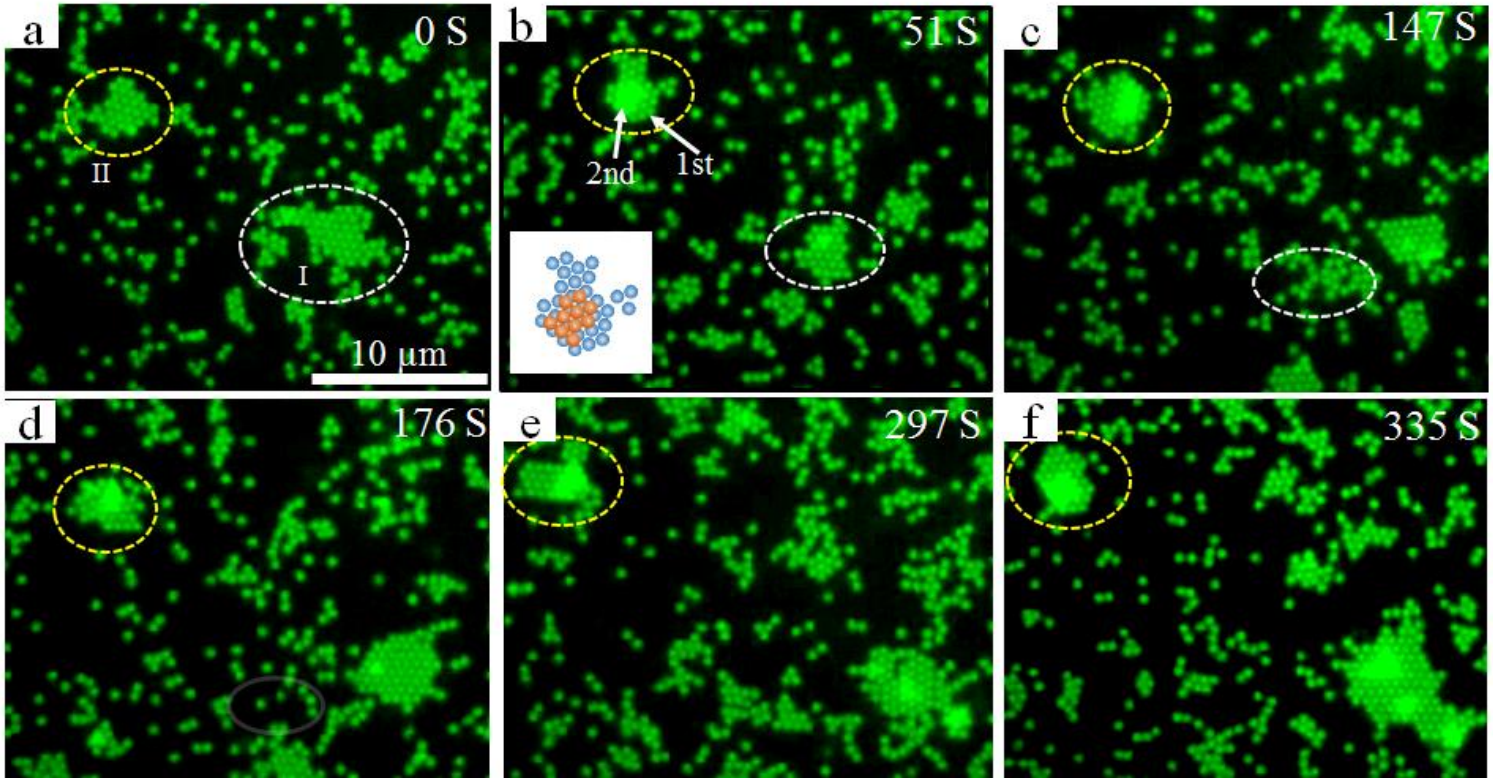

Figure 3.3 q-2D nucleation on the cover glass. The mono-layer structure enclosed in dashed white disappears, while the q-2D structure in dashed yellow (a–f) keeps growing. Inset shows a schematic of the q-2D structure.

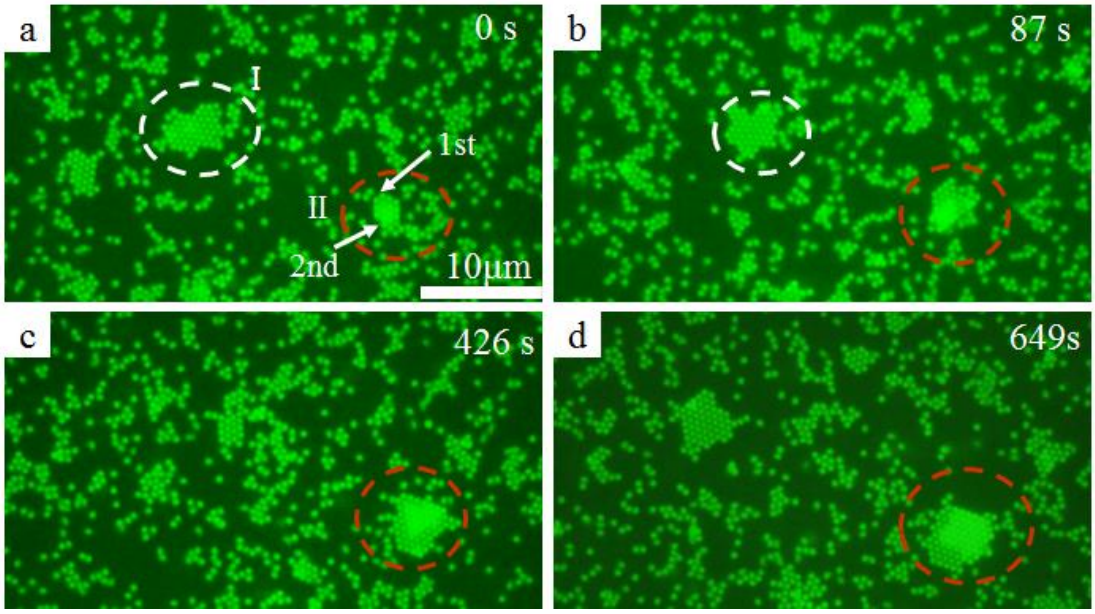

Figure 3.4 q-2D nucleation on the Pt-coated cover glass. The mono-layer structure I enclosed in dashed white disappears, while the q-2D structure II in dashed red (a–d) keeps growing.

3.1.3 Definition of surface concentration

In this study, area fraction, ϕ_{area}, is employed to represent the concentration of colloidal particles, which is defined as the area occupied by ad-particles divided by the corresponding area. We focus on the mono-layer and two-layer colloidal crystallizations. Therefore, two kinds of ϕ_{area} are defined (Figure 3.5). The area fraction of ad-particles on the substrate, ϕ^1_{area}, defined as the area occupied by ad-particles in the field of view (number of ad-particles on the substrate, $\mathcal{N}_1$, multiplied by the area of a particle, Ω), is divided by the corresponding area of a substrate (A_1-A_{grain}). The area fraction of ad-particles on the 1st layer, ϕ^2_{area}, is determined as the area of ad-particles on the 1st layer (number of ad-particles on the 1st layer, $\mathcal{N}_2$, multiplied by the area of a particle, Ω) divided by the area of the 1st layer as a terrace (A_2-A_{grain}). The area of the formed colloidal crystals is not included in the observed area in the calculation of ϕ_{area}. The number of particles in the critical nuclei on the substrate, N^*, is investigated at various ϕ^1_{area}.

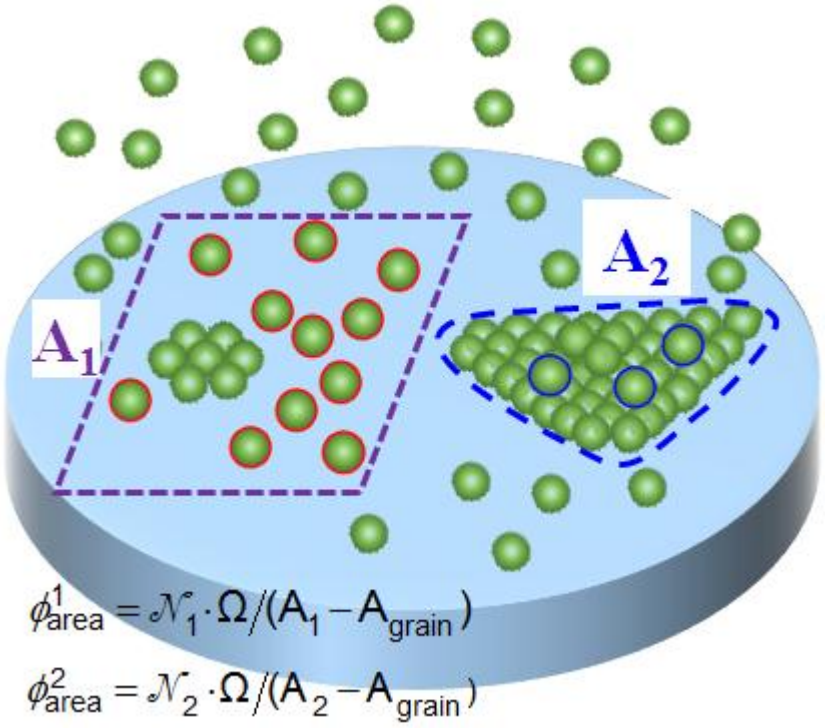

Figure 3.5 Schematic of colloidal nucleation on glass. The number of ad-particles on the substrate (red line particles) is denoted by $\mathcal{N}_1$, and that on the 1st layer (blue line particles) is denoted by $\mathcal{N}_2$. A_1 is the area chosen on the substrate (enclosed by purple dashed line), A_2 is the area of the 1st layer (enclosed by blue dashed line) and A_{grain} is the area of the grain in the chosen area. ϕ^1_{area} is the area fraction of ad-particles on the substrate. ϕ^1_{area} is the area fraction of ad-particles on the 1st layer. Ω is the area of a particle.

3.2 Critical number of particles in critical nuclei

The critical number of particles in the q-2D nuclei is obtained by measuring the minimum size of clusters that tended to grow. This is in contrast to the method for determining the number of particles in the critical mono-layer, in that the latter is obtained as the maximum size that tended to dissolve. This is due to the difficulties of observation. For q-2D islands, the frequency of disappearing embryos is significantly lower than the growing embryos. Thus, we rarely observe the disappearance of q-2D islands. In principle, the critical size is the largest size that will dissolve or the smallest size that will grow. The latter case is applied to the q-2D nucleation. The N^* in the mono-layer nuclei and q-2D nuclei are counted to be 58 and 32, respectively, at $\phi^1_{\text{area}} \approx 9\%$ in Figure 3.3. The q-2D embryo has a smaller N^* than the mono-layer embryo.

The number of particles for mono-layer and q-2D nuclei at various area fractions on the cover glass, ϕ^1_{area}, is shown in Figure 3.6. For mono-layer nucleation, as discussed above, the number of particles in the nuclei is plotted as blue circles. The blue line based on these points corresponds to the N^* at various ϕ^1_{area}. For q-2D nucleation, the number of particles in the nuclei is shown as green diamonds. The smallest value among these points is the N^* at each ϕ^1_{area}, which is shown as a green line. It is clear that N^* for the q-2D nuclei is less than that for mono-layer nuclei at a given concentration. We next investigated why N^* for q-2D nuclei is smaller than that for mono-layer nuclei in terms of the driving force required for the nucleation process in these two cases.

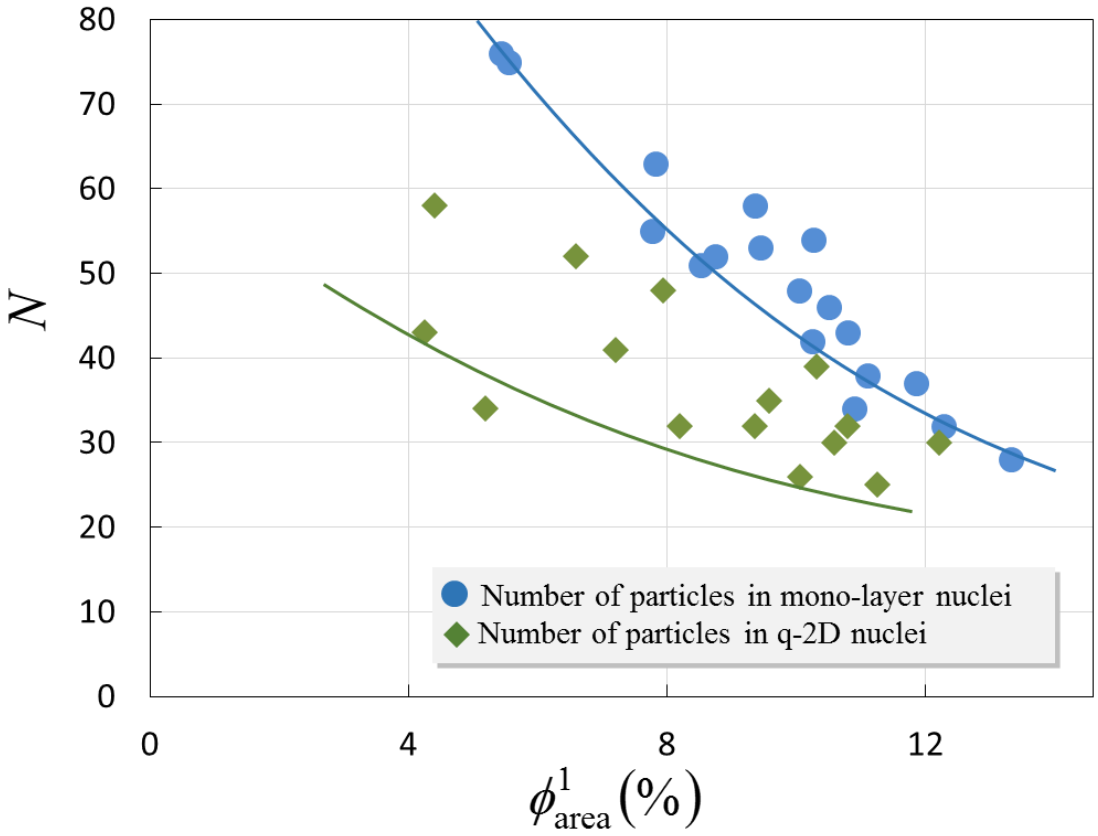

Figure 3.6 Number of particles in nucleus as a function of ϕ^1_{area} for mono-layer nuclei (blue circles) and for q-2D nuclei (green diamonds) on the substrate. The solid blue and green lines correspond to the number of particles in the critical size, N^*, for mono-layer and q-2D nuclei, respectively.

3.3 Compare ΔG of two types nucleation

Thus, the Gibbs free energy change, ΔG, for the two types of nucleation processes are evaluated here.

3.3.1 ΔG calculation for nucleation based on CNT

According to the classical nucleation theory (CNT), ΔG for forming a 3D spherical nucleus of radius r is [1]:

$$\Delta G(r) = -\frac{4\pi r^3}{3v_0}\Delta\mu + 4\pi r^2 \cdot \sigma \tag{3.1}$$

where v_0 is atomic volume, σ is the interfacial energy, and $\Delta\mu$ is the chemical potential difference between the bulk liquid and solid. There are two terms in Eq. 3.1: the decrease in volume free energy and the increase in surface free energy with the increase in r. The boundaries of all the islands are rough and the facet boundary is not observed. The rough boundary was reported for subcritical and supercritical nuclei [2–4], in which fractal dimension was calculated to obtain line tension. We have applied CNT to the rough islands assuming that islands have circular shapes with smooth boundaries. When mono-layer nuclei form on a foreign substrate, ΔG for the 2D heterogeneous nucleation, ΔG_1, in terms of number of particles, n, is expressed as

$$\Delta G_1(n) = -n\Delta\mu + \frac{2\sqrt{3}}{\pi} n\Omega \cdot \Delta\sigma + \sqrt{\frac{2\sqrt{3}}{\pi}}\pi a\sqrt{n} \cdot \gamma_1 \tag{3.2}$$

where a is the diameter of a colloid particle, Ω is the area per particle and is equal to $\pi a^2/4$, $\Delta\sigma$ is the change in interfacial free energy, and γ_1 is the step free energy (line tension) of the mono-layer nuclei. Since there are voids between particles, the constant that is derived from the area fraction of a close packed circle, $\frac{\pi}{2\sqrt{3}}$,

should be divided by the number of particles to express the area that is occupied by close packed particles and the square root of the value should be multiplied by the length of the area. Thus, $\frac{2\sqrt{3}}{\pi}$ and $\sqrt{\frac{2\sqrt{3}}{\pi}}$ are multiplied by the number of particles in the second and third terms of Eq.3.2, respectively.

Here, $\Delta\sigma$ can be expressed as

$$\Delta\sigma = \sigma_{\text{sub-solid}} + \sigma_{\text{solid-liquid}} - \sigma_{\text{sub-liquid}} \quad (3.3)$$

where $\sigma_{\text{sub-solid}}$, $\sigma_{\text{solid-liquid}}$, and $\sigma_{\text{sub-liquid}}$ are the interfacial energies between the solid/substrate, solid/liquid, and substrate/liquid interfaces, respectively.

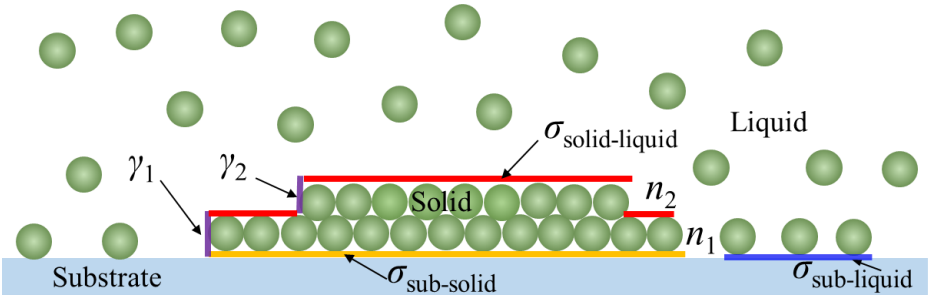

Figure 3.7 Schematic illustration of a q-2D embryo, showing parameters that are required to express the nucleation process. n_1 and n_2 are the numbers of particles of the 1st layer and the 2nd layer, respectively. γ_1 and γ_2 are the step free energies of the 1st layer and 2nd layer, respectively. $\sigma_{\text{sub-solid}}$, $\sigma_{\text{solid-liquid}}$, and $\sigma_{\text{sub-liquid}}$ are the interfacial energies of the solid/substrate, solid/liquid, and substrate/liquid interfaces, respectively.

When q-2D nuclei form on a foreign substrate, parameters for ΔG_2 are as shown in the schematic illustration of Figure 3.7. The equation for ΔG_2 is written as

$$\Delta G_2(n_1+n_2) = -(n_1\Delta\mu_1 + n_2\Delta\mu_2) + \frac{2\sqrt{3}}{\pi} n_1\Omega\cdot\Delta\sigma + \sqrt{\frac{2\sqrt{3}}{\pi}}\pi a\left(\sqrt{n_1}\gamma_1 + \sqrt{n_2}\gamma_2\right) \tag{3.4}$$

where n_1 and n_2 are the numbers of particles of the 1st layer and the 2nd layer, respectively. $\Delta\mu_1$ and $\Delta\mu_2$ are the chemical potential differences between the solution and the 1st layer, and the solution and the 2nd layer, respectively, at a certain supersaturation. γ_1 and γ_2 are the step free energies (line tensions) of the 1st layer and 2nd layer, respectively.

For a given interparticle interaction, $\Delta\mu$ can be expressed in terms of the supersaturation δ [5]:

$$\Delta\mu = k_B T \ln(1+\delta) \tag{3.5}$$

where k_B is Boltzmann's constant and T is the absolute temperature. δ is related to the actual concentration (C) and equilibrium concentration (C_{eq}). Assuming C and C_{eq} correspond to ϕ_{area} and equilibrium area fraction, ϕ_{eq}, δ is expressed by

$$\delta = \frac{\phi_{area} - \phi_{eq}}{\phi_{eq}} \tag{3.6}$$

Substituting Eqs. 3.5 and 3.6 into Eq. 4, ΔG_2 is expressed as

$$\begin{aligned}\Delta G_2(n_1+n_2) = -\left(n_1 k_B T \ln\left(\phi^1_{area}/\phi^1_{eq}\right) + n_2 k_B T \ln\left(\phi^2_{area}/\phi^2_{eq}\right)\right) \\ + \frac{2\sqrt{3}}{\pi} n_1\Omega\cdot\Delta\sigma \\ + \sqrt{\frac{2\sqrt{3}}{\pi}}\pi a\left(\sqrt{n_1}\gamma_1 + \sqrt{n_2}\gamma_2\right)\end{aligned} \tag{3.7}$$

where ϕ^1_{eq} and ϕ^2_{eq} are the equilibrium area fractions of the colloidal particles on the 1st layer and 2nd layer, respectively. Among the parameters in Eq. 3.7, ϕ^2_{eq} and

γ_2 were obtained from Nozawa et al. [6]. To calculate ΔG_2, the following parameters should be obtained: ϕ^1_{eq}, $\Delta\sigma$, and γ_1.

3.3.2 Measuring equilibrium concentration (ϕ^1_{eq}) on the cover glass

Here, the equilibrium concentration on the cover glass, ϕ^1_{eq}, is determined. ϕ^1_{eq} is measured experimentally as ϕ^1_{area} at which the growth rate of steps of the 2D island is zero assuming that $\Delta\mu$ is used only for growth kinetics. As nuclei grow, particles in the solution are consumed, leading to a decrease in supersaturation. Therefore, step velocity becomes small as time proceeds. The step velocity is close to 0 when ϕ^1_{area} becomes close to ϕ^1_{eq}. The particles begin to dissolve when ϕ^1_{area} is smaller than ϕ^1_{eq}. The step velocity is determined as following. Figure 3.8 (a) shows the grains grown in the colloidal suspensions. The step growth of one grain was traced from the movement as it grows in different directions, as illustrated in Figure 3.8 (b). The step velocity is calculated along the directions indicated by arrows based on the data of Figure 3.8 (b). Then, the average value of the step velocity in different directions is used to determine the relationship between the step velocity and ϕ_{area} on the substrate, as presented in Figure 3.8 (c). The results show that ϕ^1_{eq} is determined to be about 1.1%.

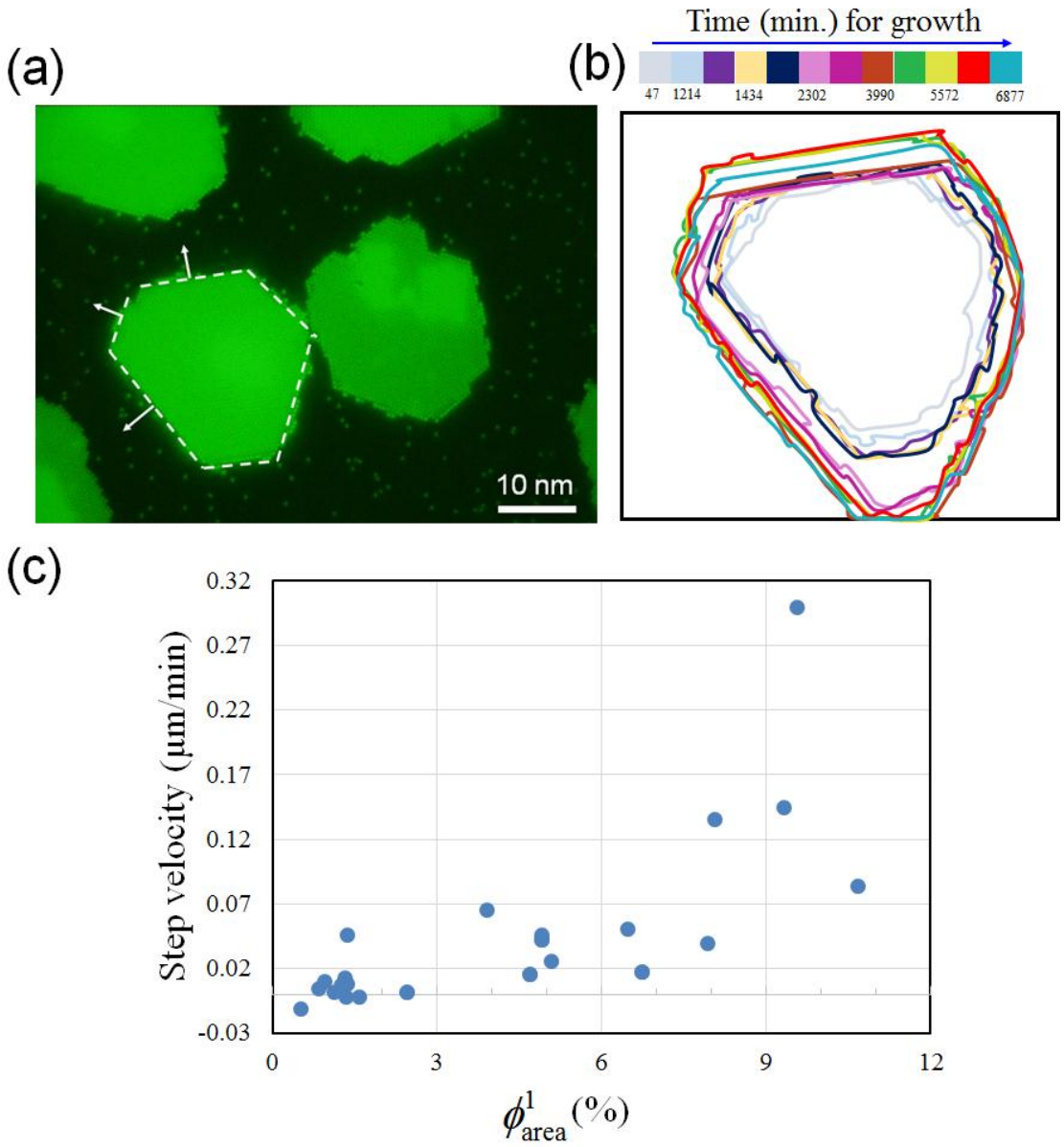

Figure 3.8 (a) Growth of a grain in the colloidal suspension. Dashed lines represent the step of one grain, and arrows indicate the growth direction of the grain. (b) Tracing the step of the 1st layer in the grain with time. (c) Step velocity versus ϕ^1_{area}.

3.3.3 Interfacial energy change ($\Delta\sigma$) and line tension (γ) on the cover glass

$\Delta\sigma$ and γ_1 are also measured experimentally based on the CNT of mono-layer nucleation, in which these parameters determine the critical number of particles, N^*. N^* is obtained by differentiating Eq. 3.2 and setting it equal to zero as

$$\frac{d\Delta G_1(n)}{dn} = -\Delta\mu + 1.1\Omega\Delta\sigma + 1.05\pi a\gamma_1 \frac{1}{2\sqrt{n}} = 0 \quad \text{at } n = N^* \tag{3.8}$$

Then,

$$\frac{1}{\sqrt{N^*}} = \frac{2k_B T}{1.05\pi a\gamma_1} \ln\left(\phi^1_{\text{area}} / \phi^1_{\text{eq}}\right) - \frac{1.1a\Delta\sigma}{2\times 1.05\gamma_1} \tag{3.9}$$

by replacing Ω with $\pi a^2/4$.

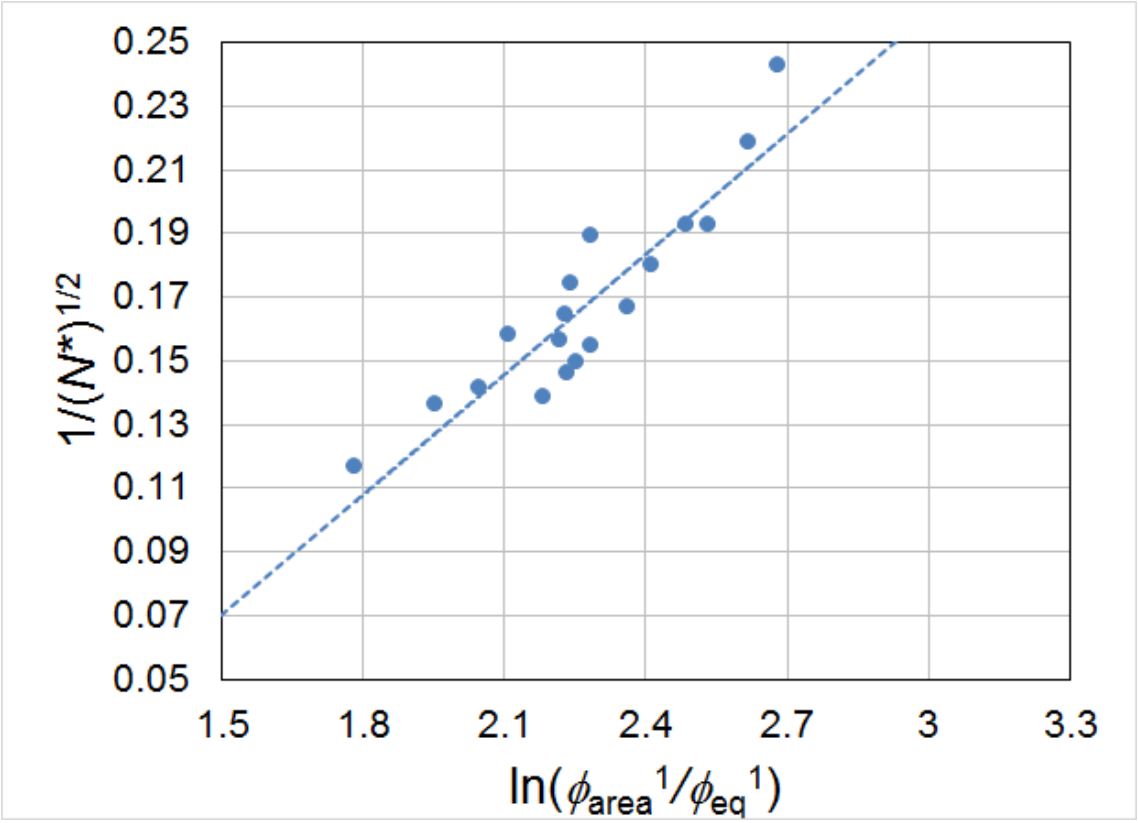

Figure 3.9 Reciprocal of the square root of the critical size, $1/\sqrt{N^*}$, as a function of $\ln\left(\phi_{\text{area}}^{1}/\phi_{\text{eq}}^{1}\right)$.

The number of particles for the critical mono-layer nuclei is obtained at various ϕ^1_{area} (Figure 3.6). The reciprocal of the square root of the critical size, $1/\sqrt{N^*}$, as a function of $\ln\left(\phi^1_{\mathrm{area}}/\phi^1_{\mathrm{eq}}\right)$ is shown in Figure 3.9. The fitting line is drawn without taking into account several unreliable data points that deviated significantly from the trend of the other data. $\Delta\sigma$ and γ_1 are derived as 1.1 $k_{\mathrm{B}}\mathrm{T}/a^2$ and 4.6 $k_{\mathrm{B}}T/a$, respectively. In a hard sphere system, the value of $\Delta\sigma$ on the hard-wall is obtained by computer simulation as almost zero.[31] Since there are interactions between particles and substrate, $\Delta\sigma$ obtained from the experiments shows a non-zero value. The step free energy of the 1st layer, γ_1, is five times larger than that of the hard-sphere system [7] and almost the same as that of the 2nd layer [6]. This increment is thought to be the sum of interactions between particles as well as between particles and substrate.

In general, although $\Delta\sigma$ is an important parameter for nucleation such as epitaxial growth, it is very difficult to measure the critical nucleus in an atomic system. In contrast, observations at single-particle resolution of colloidal crystals are easy, which enables us to measure the critical size.

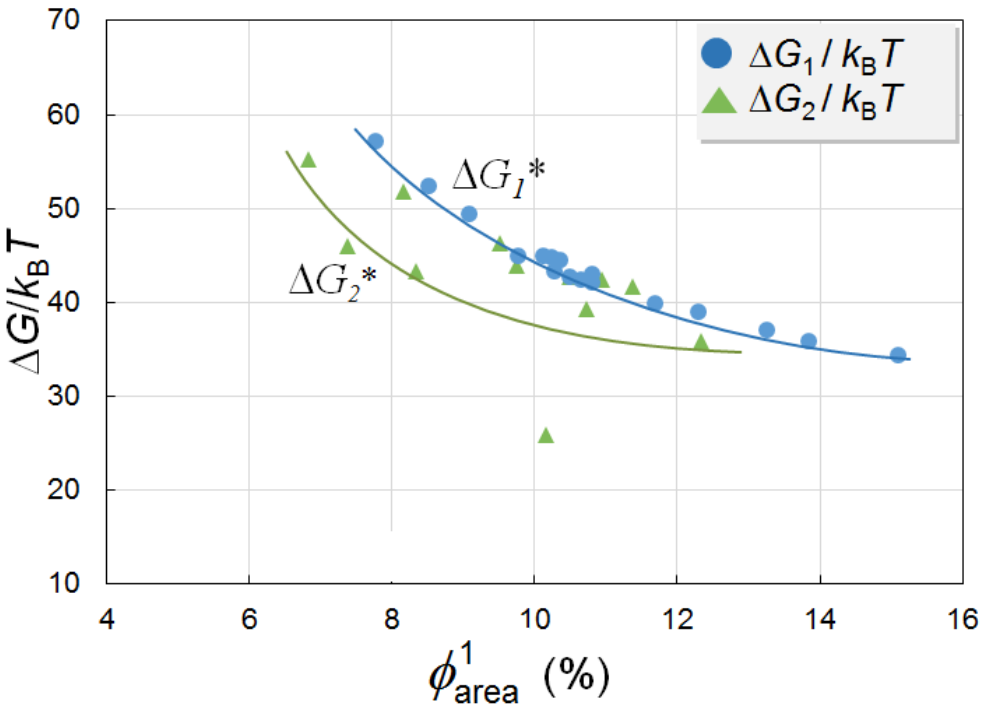

Figure 3.10 Gibbs free energy, ΔG, for mono-layer nucleation, ΔG_1, and that for q-2D nucleation, ΔG_2, at various ϕ^1_{area}. The solid blue and green lines correspond to the critical Gibbs free energy change, ΔG^*, for mono-layer and q-2D nucleation, respectively.

All the parameters, ϕ_{eq}^{1}, ϕ_{eq}^{2}, γ_1, γ_2, and $\Delta\sigma$, are substituted into Eq. 3.4 and Eq. 3.7 for each point in Figure 3.6. The ΔG of mono-layer nuclei, ΔG_1, and two-layer nuclei, ΔG_2, at various area fractions are calculated as shown in blue circles and green triangles, respectively, in Figure 3.10. The blue and green lines based on these points are the minimum ΔG, which corresponds to the ΔG^* at various ϕ_{area}^{1}.

These calculations suggest that ΔG^* for q-2D nucleation is smaller than that for mono-layer nuclei at the same ϕ_{area}^{1}. This explains our experimental results shown in Figure 3.6 in which nucleation occurs with a smaller number of particles for q-2D nuclei than for mono-layer ones.

Although q-2D nucleation has a smaller ΔG, mono-layer nucleation is predominant when ϕ_{area}^{1} is larger than 12%. There is no q-2D nucleation observed in the ϕ_{area}^{1} range over 12% in Figures 3.6 and 3.10. This is explained by the induction time of the second layer formation. For q-2D nucleation, a certain time is required to form the 2nd layer. On the other hand, at high ϕ_{area}^{1}, mono-layer nucleation occurs very quickly and consumes particles for growth, which decreases ϕ_{area}^{1}. Therefore, even though q-2D nucleation has a smaller ΔG, it is prevented kinetically.

In Figure 3.10, the parameter to express the quantity of the particles in the 2nd layer relative to those of the 1st layer is not included. Figure 3.11 shows the effect of the secondary layer on ΔG, in which the axis of n_2/n_1 is added, and the color contrast represents the value of ΔG. When n_2/n_1 equals zero, i.e., a mono-layer nucleus, blue circles in Fig. 3.11 correspond to those in Fig. 3.10.

When n_2/n_1 is larger than zero, ΔG_2 decreases with increasing n_2. The appearance of the 2nd layer for q-2D nuclei reduces the interface between crystal and substrate, decreasing ΔG for the nucleation of particles. In other words, since formation of colloidal layers on the glass substrate is not as favorable as formation on the surface of colloidal crystals as a secondary layer (measured by $\Delta\sigma$), nucleation with two layers is the lower path to overcome the energetic barrier for nucleation at a given number of particles.

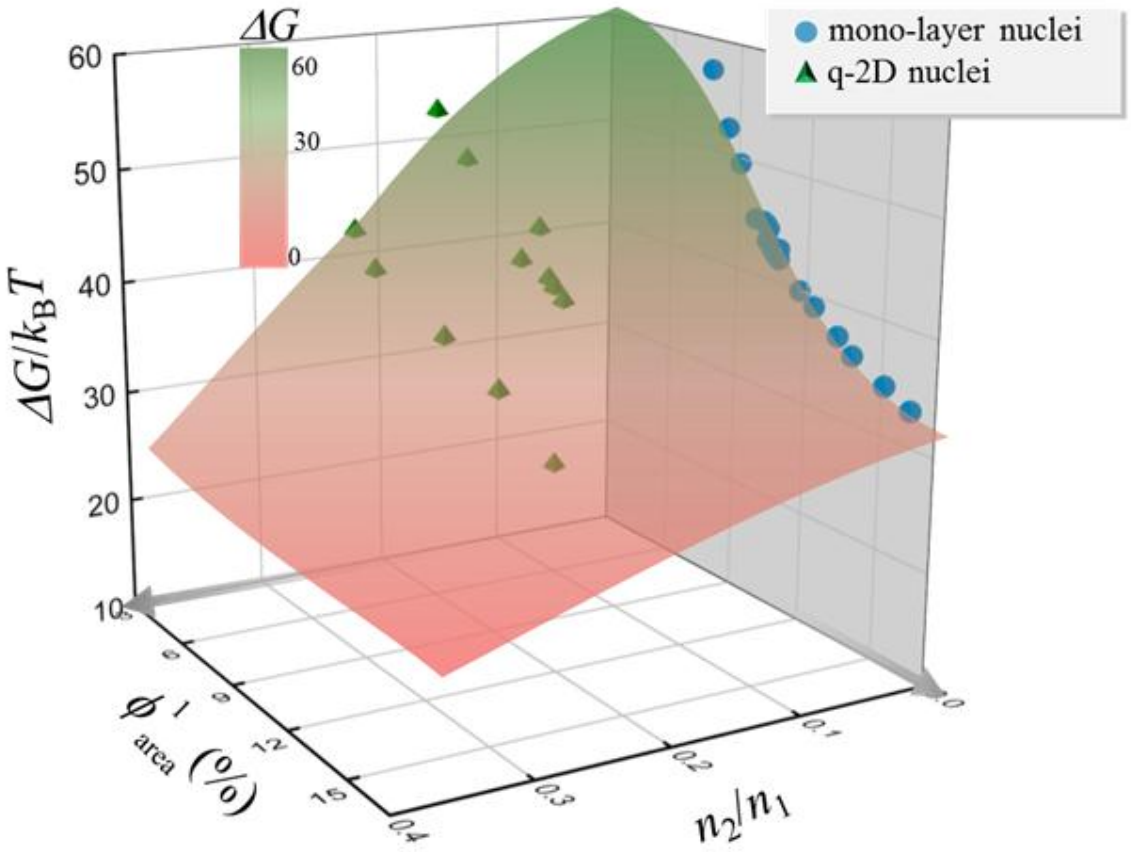

Figure 3.11 Plots of ΔG versus ϕ^1_{area} and n_2/n_1. Blue circles correspond to mono-layer nuclei, and green diamonds represent q-2D nuclei. The colored surface shows ΔG of nuclei formation as a function of ϕ^1_{area} and n_2/n_1.

3.4 Summary

Heterogeneous nucleation of colloidal crystals on a glass substrate has been investigated by *in situ* observations. Two types of nucleation processes were observed: mono-layer and q-2D nucleation. Interfacial free energy change, $\Delta\sigma$, and step free energy of the 1st layer, γ_1, were obtained from measurements of the critical size of nuclei and analysis based on the classical nucleation theory (CNT) equation. The ΔG calculations suggest that ΔG of q-2D nucleation is smaller than that for mono-layer nucleation at a given ϕ_{area}^{1}, which explains the experimental results that N^* for q-2D nuclei is smaller than that for mono-layer nuclei. We have succeeded in quantitatively examining the substrate effect as $\Delta\sigma$ via the nucleation process. Since $\Delta\sigma$ are important parameters for controlling the size and shape of colloidal nuclei, our findings will contribute to wide fields of applications of colloidal crystals such as colloidal epitaxy and lithography.

References

[1] D. A. Porter, K. E. Easterling, M. Y. Sherif. *Phase Transformations in Metals and Alloys*, 3rd ed. (Revised Reprint), CRC press, 2009, Chapter 4, pp182–190.

[2] A. E. González, I. C. Leonardo. Fractal Structure of the Crystalline-nuclei Boundaries in 2D Colloidal Crystallization: Computer Simulations. *Phys. Lett. A* **2012**, 376, 1375–1379.

[3] A. E. González. Colloidal Crystallization in 2D for Short-Ranged Attractions: A Descriptive Overview. *Crystals* **2016**, 6, 46.

[4] P. Dillmann, G. Maret, P. Keim. Two-dimensional Colloidal Systems in Time-dependent Magnetic Fields. *Eur. Phys. J. Spec. Top.* **2013**, 222, 2941–2959.

[5] R. H. Fowler, E. A. Giggenhein, *Statistical Thermodynamics*; Cambridge Univ. Press, London, **1960**.

[6] J. Nozawa, S. Uda, S. X. Guo, S. M. Hu, A. Toyotama, J. Yamanaka, J. Okada and H. Koizumi. Two-Dimensional Nucleation on the Terrace of Colloidal Crystals with Added Polymers. *Langmuir* **2017,** 33(13), 3262–3269.

[7] S. Auer, D. Frenkel. Line tension controls wall-induced crystal nucleation in hard-sphere colloids. *Physical review letters*, **2003**, 91(1), 015703-1–4.

Chapter 4 Effect of substrate on nucleation rate of two-dimensional colloidal crystals

In Chapter 3, the effect of the substrate was found to be important for the heterogeneous nucleation of colloidal crystals. As introduced in Chapter 1, $\Delta\sigma$ affects the nucleation and growth in the atomic system. To investigate the effect of substrate on nucleation in the colloidal system, different types of substrates are applied. In this chapter, three types of substrates are used and the consequent effect on the nucleation rate, J, is examined.

4.1 Nucleation on three substrates

After mixing the polymer solution and suspension, the particle concentration on the substrate gradually increases due to sedimentation of the particles by gravity and the depletion attraction between the particles and substrate which is induced by overlap of the depletion zones. Since 500 nm colloidal particles display strong Brownian motion, particles that do not form clusters return to solution after diffusion on the substrate. When the particle concentration reaches a certain value, nucleation occurs on the substrate. Figure 4.1 shows the nuclei formed 15 min. after starting the experiment for the three different substrates under the same initial volume fraction, Φ. Some clusters with sizes less than the critical size will dissolve into the solution. Conversely, some that surpass a critical size will continue to grow. Most of the nucleation occurs as monolayer (2D) nucleation. Repeating the 2D nucleation on the terrace, these nuclei grow into colloidal crystals with 3–5 layers. Among the three substrates, the number of nuclei on the uncoated cover glass is largest while it is smallest for the Pt-coated cover glass. Thus, it is clear that the nucleation rate is dependent on the substrate material.

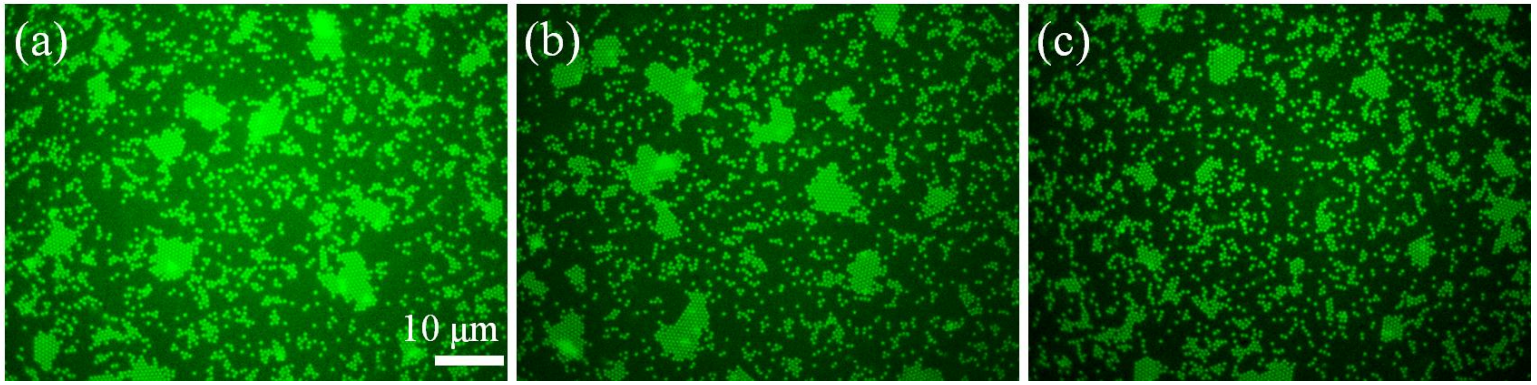

Figure 4.1 Nucleated 2D islands on different substrates, cover glass (a), Au-coated cover glass (b) and Pt-coated cover glass (c), under the same solution conditions, where Φ is 0.5% and the concentration of sodium polyacrylate is 0.15 g/L.

4.2 Nucleation rate (J) on different substrates

The heterogeneous 2D nucleation rate can be measured via in situ observation. This measurement is expressed as shown in eq. 4.1.

$$J = \frac{N}{S\Delta t} \tag{4.1}$$

where N is the number of nuclei in the observed region, S is the observed area, and Δt is a certain time interval in the nucleation process. Figure 4.2 shows the number of nuclei and ϕ_{area} as a function of time. Based on eq. 4.1, J is summarized at various ϕ_{area} in Figure 4.3.

The relationship between nucleation rate, J, and area fraction, ϕ_{area}, which is introduced as the surface concentration of particles, for the three substrates is investigated. Figure 4.3 shows the J of 2D colloidal crystals as a function of ϕ_{area} for three different substrates. Details of the measurement of J are discussed in the Supplementary section. Among the three substrates, cover glass has the largest J while the Pt-coated substrate has the smallest J under the same ϕ_{area}.

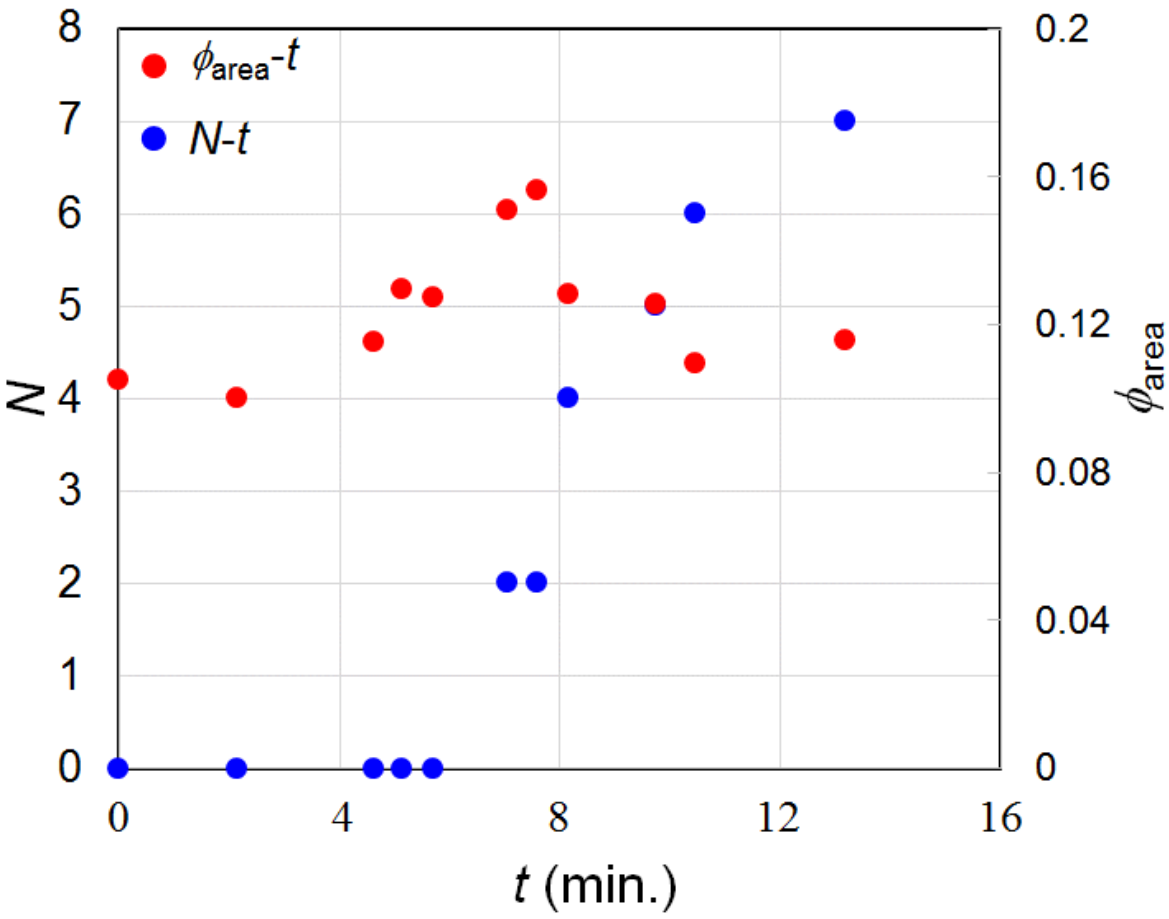

Figure 4.2 Variation of the number of grains, N, and ϕ_{area} with time. Red circles represent the values of ϕ_{area} on the substrate, whereas blue ones represent N in the suspension.

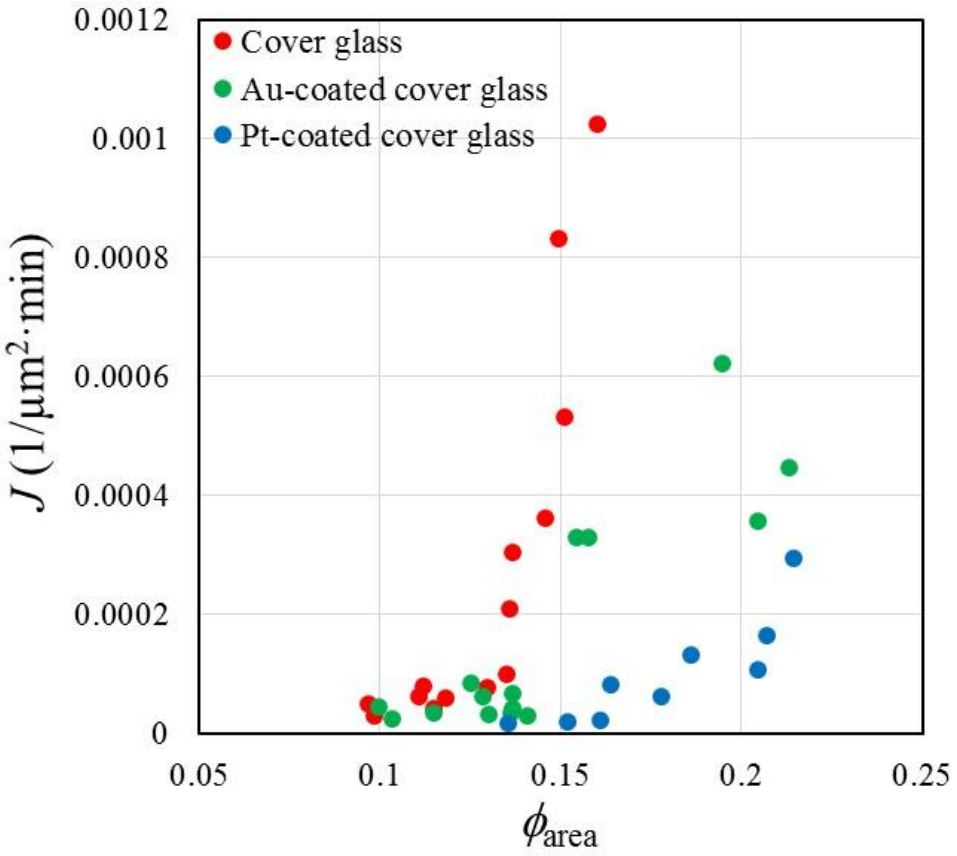

Figure 4.3 The nucleation rate, J, at various ϕ_{area} for three different substrates.

4.2.1 Derivation of *J*

We next analyzed the difference in J for different substrates from the thermodynamic viewpoint. In our previous work, the Gibbs free energy change, ΔG, for 2D nucleation was expressed in terms of the number of particles, n, taking the interfacial energy change, $\Delta\sigma$, into account [1],

$$\Delta G\ (n) = -n\Delta\mu + \frac{2\sqrt{3}}{\pi} n\Omega \cdot \Delta\sigma + \sqrt{\frac{2\sqrt{3}}{\pi}} \pi a \sqrt{n} \cdot \gamma \tag{4.2}$$

where a is the diameter of a colloid particle, Ω is the area per particle (equal to $\pi(a/2)^2$), γ is the step free energy (line tension) of nuclei, and $\Delta\mu$ is the chemical potential difference between the bulk liquid and solid. Here, $\Delta\mu$ is a function of supersaturation, which is expressed as $(\phi_{\text{area}} - \phi_{\text{eq}})/\phi_{\text{eq}}$, where ϕ_{eq} is the equilibrium concentration. The $\Delta\sigma$ is the change in interfacial free energy, which is given by

$$\Delta\sigma = \boldsymbol{\sigma}_{\text{sub-solid}} + \sigma_{\text{solid-liquid}} - \sigma_{\text{sub-liquid}} \tag{4.3}$$

where σ is the interfacial energy between each phase. The critical Gibbs free energy change, ΔG^*, of the formation of critical nuclei leads to [1]

$$\Delta G^* = \frac{\sqrt{3}\pi a^2 \gamma^2}{2\Delta\mu - \sqrt{3}a^2\Delta\sigma} \tag{4.4}$$

and J is expressed as

$$J = A\exp\left(-\frac{\Delta G^*}{k_B T}\right) \tag{4.5}$$

where k_B is the Boltzmann constant, T is the absolute temperature, and A is a kinetic prefactor that is related to the attachment rate of the particles surrounding the critical nuclei, the Zeldvich factor, and the number density of the colloidal particles.

Substituting eq. 4.4 into the above equation yields

$$\ln J = \ln A - \frac{\sqrt{3}\pi a^2 \gamma^2}{(2k_B T \ln \phi_{area} / \phi_{eq} - \sqrt{3}a^2 \Delta\sigma) k_B T} \quad (4.6)$$

Here, the ϕ_{eq} is determined experimentally as ϕ_{area} where the growth rate of steps of 2D islands is zero, assuming that $\Delta\mu$ is only used for growth kinetics. The ϕ_{eq} for cover glass, Au-coated and Pt-coated cover glass are 1.1, 0.9 and 0.95%, respectively.

4.2.2 Interfacial energy change ($\Delta\sigma$) from the experimental

The values in Figure 4.3 are replotted based on eq. 4.6 as shown in Figure 4.4. The $\Delta\sigma$ is obtained from Figure 4.4 by fitting eq. 4.6. The values of $\Delta\sigma$ on the cover glass, Au-coated, and Pt-coated cover glass are determined to be 0.83, 1.39, and 1.47 [$k_B T/a^2$], respectively.

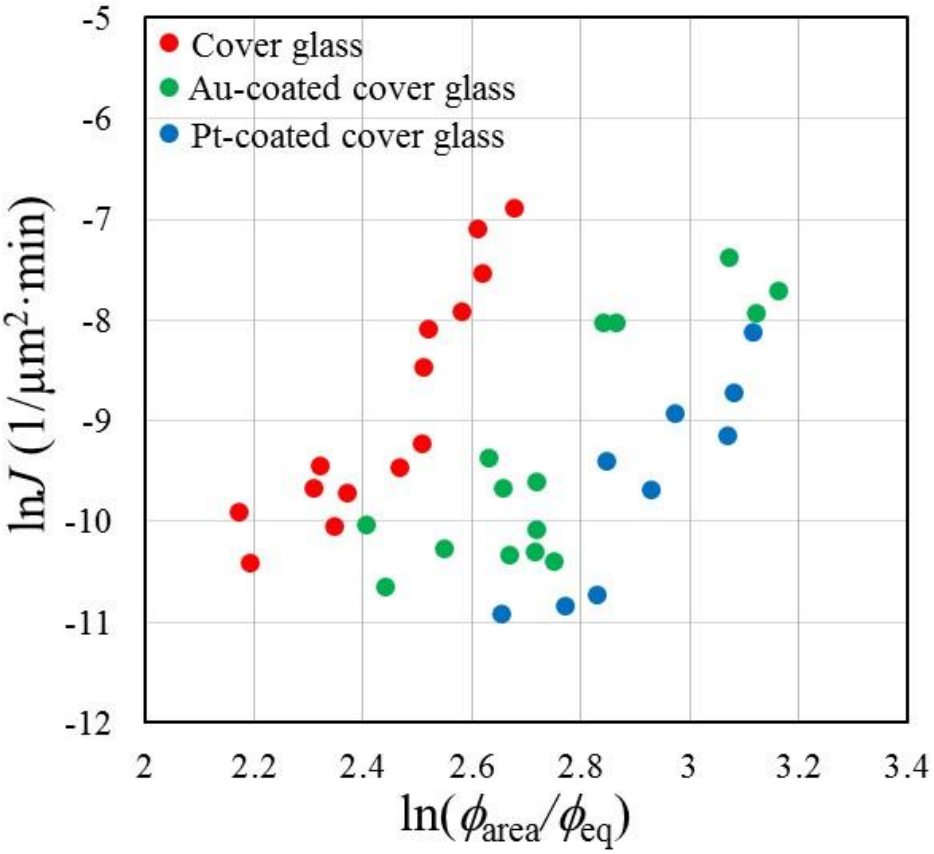

Figure 4.4 The ln$J$ as a function of ln(ϕ_{area}/ϕ_{eq}) for three different substrates.

4.3 Interaction between PS particles and substrate

In the atomic system, $\Delta\sigma$ is dependent on the bonding energy between the substrate and a formed crystal. We deduce that the $\Delta\sigma$ for colloidal crystals is related to the strength of the interaction between particles and the substrate. The interaction between particles and substrate in a polymer solution mainly consists of the depletion attraction and the vdW force. The vdW force plays the dominant role for the interaction between submicron-sized particles and substrate, e.g., the adsorption of a silica particle onto hydrogel surfaces is driven by the vdW force. [2] Since the strength of the depletion attraction depends on the size and density of the polymers, [1] its value is independent of the substrate material, while the magunitude of the vdW force is dependent on the material. Therefore, to determine the vdW force between particles and each substrate, surface force measurements were conducted in pure water. The surface force measurement is a powerful method to measure very slight forces interacting between two substances with high sensitivity. [3–5] All of the surface force measurements in this study were conducted in pure water instead of polymer added water. Since polymers easily adhere to the cantilever of the AFM, the measurement was challenging. However, because the depletion attraction is the same for all three substrates, the order of interaction between the particle and each substrate corresponds to that of the vdW force interaction.

4.3.1 Surface force measurement

The surface force between a colloidal particle and a substrate was measured by an atomic force microscope (AFM) equipped with a colloidal probe. The colloidal probe was prepared by gluing a polystyrene (PS) particle of 10 μm

in diameter at the tip of a cantilever (Figure 4.5). The interaction force, F, was measured as the product of the spring constant of the cantilever, k, and deflection of the cantilever. The deflection of the cantilever was measured from the laser position that was reflected from the back of the cantilever and monitored by a position-sensitive sensor (four-sectored photodiode). The surface separation (D) was measured by a piezoelectric device.

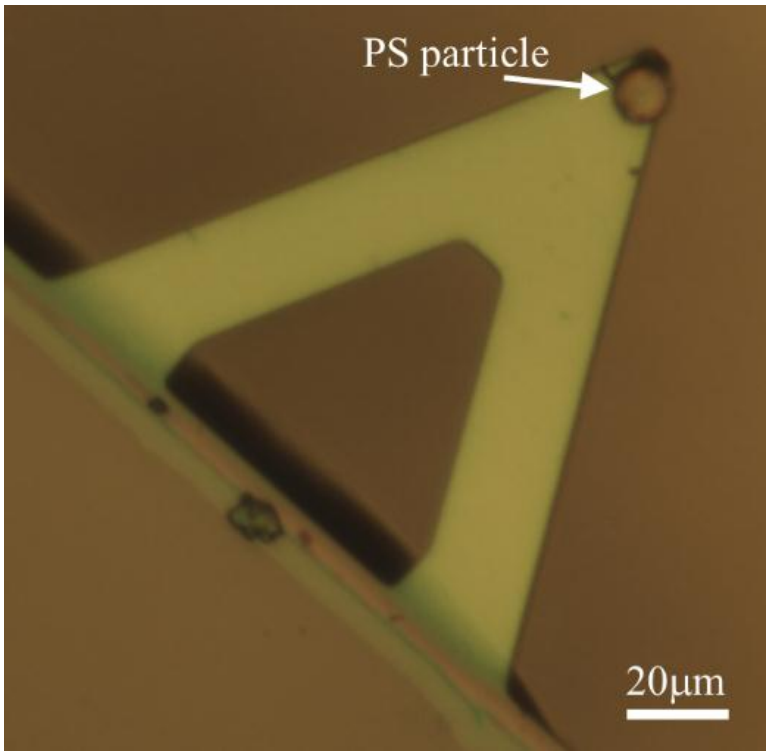

Figure 4.5 Optical microscopy image of colloidal probe cantilever. The white arrow indicates the PS particle.

The k is calculated from resonant frequency, [6]

$$k = (2\pi)^2 \frac{M_1}{(1/\nu_1^2 - 1/\nu_0^2)} \tag{4.7}$$

where ν_1 is the unloaded resonant frequency before the PS particle was attached, and ν_1 is the resonant frequency with the added mass of the PS particle M_1. All measurements were conducted with one cantilever, and the value of k was determined to be 0.383 N/m.

The measurement consists of two processes, approach of the substrate to the PS particle and separation from it. The profiles of the interaction force as a function of the distance between the PS particle and substrate were obtained. At the beginning of the approach process, the cantilever remained undeflected over the 1000 nm range (See Figure 4.6 (a)). The repulsive interaction was detected within the distance of 200 nm. The tip of the cantilever jumped into contact with the substrate when the attractive force exceeded the stiffness of the cantilever. The substrate was further pushed towards the cantilever until the force and distance showed a linear relationship, from which the zero distance and the sensitivity of the cantilever were determined. In the separation process, the tip jumped out from the substrate when the elastic force of the cantilever surpassed the adhesive force between the particle and substrate.

The measurements were taken at least 10 consecutive times. The obtained forces (F) were normalized by the radius (R) of the colloidal sphere using the Derjaguin approximation, [7] $F/R = 2\pi G_f$, where G_f is the interaction free energy per unit area between two flat surfaces. R is measured from the optical microscopy images.

4.3.2 Compare the order of experimental results of interaction between PS particles and substrate with that of calculation

Figure 4.6 (a) shows the force-distance profiles for the PS particle and three substrates in pure water measured during the approach process. The adhesive forces measured in the separation process are indicated at zero distance. The details of the measurements are described in the Supporting Information. Repulsive forces are observed in the distance range from several tens to 100 nm for all of the substrates, which are due to the electrostatic repulstion between the particle and substrates. As the substrate approaches the PS particle, the PS particle jumps into contact with the substrate, which is called "jump-in," indicating that the gradient of the attractive force (vdW attraction) exceeds the stiffness of the cantilever. The jump-in is observed for all three substrates. After the approach process, the forces on the separation process are also measured, and "jump-out" is observed. The adhesive forces are determined as the force required for the jump-out to take place. The adhesive force consists of an electrostatic repulsion and the vdW force. However, since the vdW force is dominant at short distances, we regard the order of adhesive force for the three substrates as that of the vdW attraction. The adhesive forces for each substrate are shown in Figure 4.6 (b). The adhesive force for Pt-coated cover glass is the largest while that for the uncoated cover glass is the smallest. This magnitude order is the same as that for the $\Delta\sigma$ values for each substrate determined from J. It is thus demonstrated that $\Delta\sigma$ is based on the interaction between the particle and the substrate.

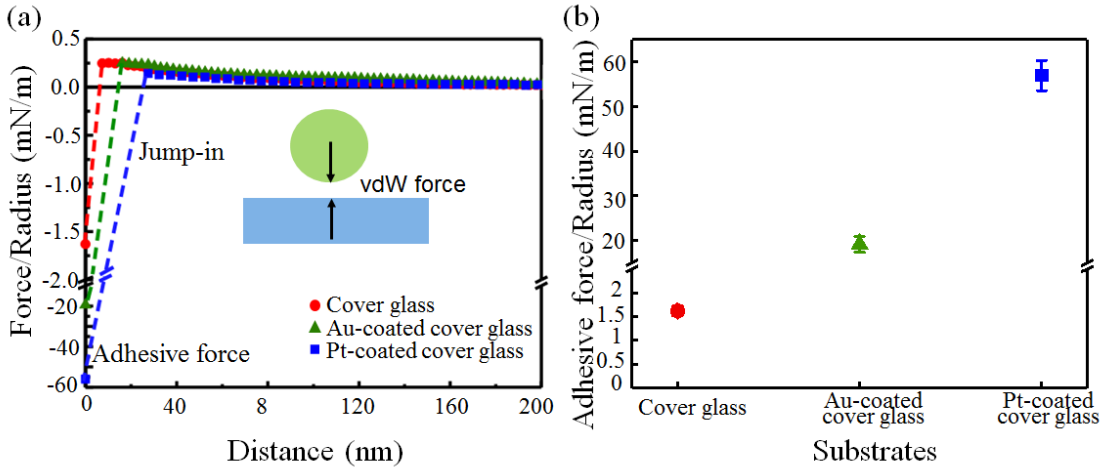

Figure 4.6 (a) Force–distance profiles between polystyrene particle and each substrate in pure water. A positive sign of the force corresponds to a repulsive interaction while a negative sign indicates an attractive force. Dashed lines indicate when the particle jumps into contact. Inset illustration shows the vdW force between the particle and substrate. (b) Statistics of adhesive forces between colloidal particles and three kinds of substrates. Red circles represent the value for cover glass, green triangles for Au-coated cover glass and blue squares for Pt-coated cover glass.

In general, the vdW force can also be estimated by calculations using the Hamaker constant of individual materials. The vdW force between particles and a plate is given by [8]

$$F_{\mathrm{vdW}} = -\frac{A_{\mathrm{H}} R}{6D^2} \tag{4.8}$$

where A_{H} is the Hamaker constant between a colloidal particle and a plate in a solution medium, R is the radius of one colloidal particle, and D is the distance between the particle surface and a plate. A_{H} is calculated using individual Hamaker constants of polystyrene, water and each substrate as, [8]

$$A_{\mathrm{H}} = (\sqrt{A_{11}} - \sqrt{A_{22}})(\sqrt{A_{33}} - \sqrt{A_{22}}) \tag{4.9}$$

where A_{11}, A_{22}, and A_{33} are the Hamaker constants of the colloidal particle, water, and substrate, respectively. The following values are used for the calculations: polystyrene, $A_{11} = 6.6\times10^{-20}$ J; [8] water, $A_{22} = 3.7\times10^{-20}$ J; [9] glass, Au and Pt, $A_{33} = 6.3\times10^{-20}$, 38×10^{-20} and 20×10^{-20} J, respectively. [10] The combined Hamaker constants of eq. 7 for cover glass, Au-coated and Pt-coated cover glass are calculated to be 0.4×10^{-20}, 2.7×10^{-20} and 1.6×10^{-20} J, respectively. The combined Hamaker constant, $\Delta\sigma$ and adhesive forces for the three substrates are summarized in table 4.1.

Table 4.1 The values of combined A_H, adhesive forces and $\Delta\sigma$ on three substrates

Substrates	A_H (10^{-20}J)	Adhesive force (mN/m)	$\Delta\sigma$ (k_BT/a^2)
cover glass	0.4	1.61±0.10	0.83
Au	2.7	19.12±1.77	1.39
Pt	1.6	56.93±3.38	1.47

Among the three substrates, the calculated van der Waals interaction between PS particles and Au-coated cover glass is the largest. This is not consistent with the surface force measurements and $\Delta\sigma$ values determined from J. This inconsistency is likely caused by the roughness of the coated substrate since the vdW force is dependent on roughness [11]

4.3.3 The effect of substrate roughness on the interaction between PS particles and substrate

We then conducted the surface force measurements for different substrates with similiar roughness. The average surface roughnesses on Au-coated and Pt-coated cover glass that are used in the nucleation experiment are measured by AFM to be 0.84 ± 0.08 and 0.29 ± 0.04 nm. The roughness of the Pt-coated cover glass is smaller than that of the Au coating. Thus, the surface force measurements for different substrates with approximately the same roughness were conducted. The adhesive force of Pt-coated cover glass with a roughness of 1.11 ± 0.06 nm was compared to that of Au with nearly the same roughness (0.84 ± 0.08 nm). The adhesive force of the Pt-coated cover glass is measured to be 17.30 ± 1.25 mN/m (force profile is shown in Figure 4.7), which is less than that of the Au-coated cover glass. The greater roughness of the substrate yields less adhesive force, which is suggested by the relationship between the strength of the vdW force and roughness. [11] If the influence of roughness is taken into account, the order of measured forces is in accordance with the calculation results based on eq. 4.8 for the coated samples.

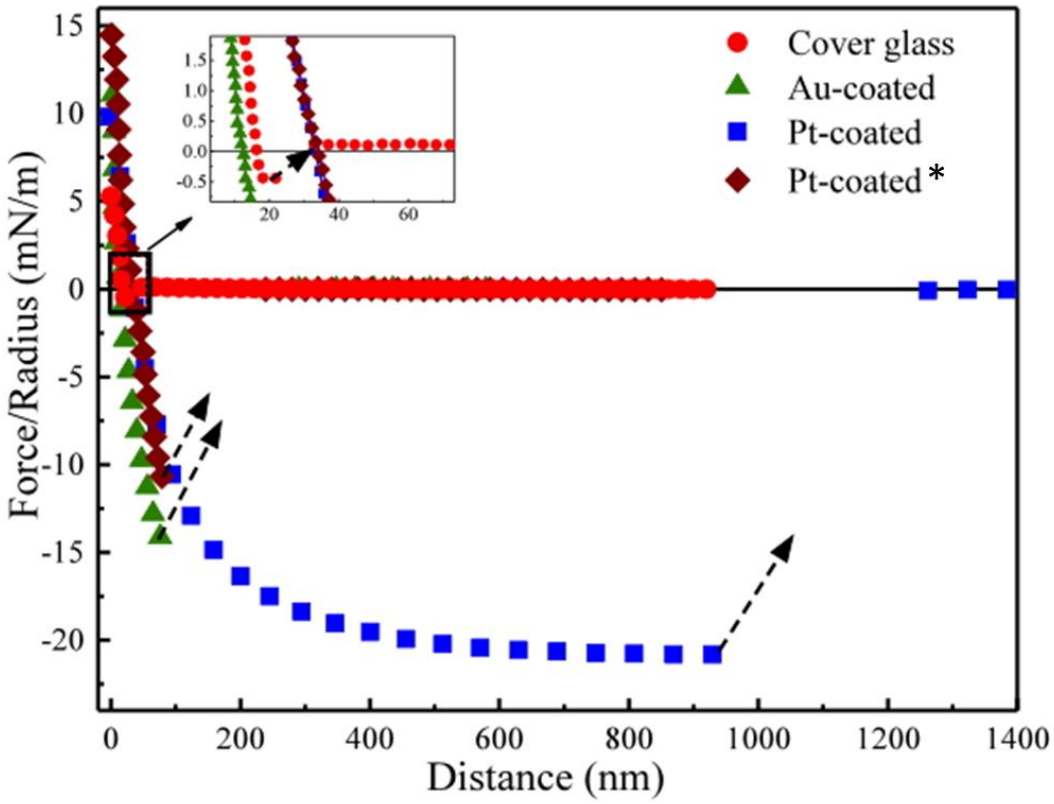

Figure 4.7 Force profiles of interactions between PS particles and substrates upon separation. Red circles represent plots for the cover glass, green triangles for the Au-coated cover glass, blue squares for the Pt-coated cover glass (roughness of 0.29 ± 0.04 nm) and brown diamonds for Pt-coated* cover glass with a different roughness (1.11 ± 0.06 nm). The inset figure shows an enlargement of the short distance range. The dotted arrows show where the cantilever jumped out from contact with the substrate.

Here, it should be noted that, to our knowledge, this is the first time that surface force measurements between polystyrene colloidal particles and Au and Pt films over water medium have been conducted. These results are applicable to not only colloidal crystallization, but also to various surface chemistry fields that include surfaces of polystrene, Au or Pt.

We have studied the effect of substrates on the J of 2D colloidal crystals. The value of $\Delta\sigma$ is relevant to the strength of the interaction between particles and substrates. We demonstrated that $\Delta\sigma$ for colloidal crystals could be controlled by changing the substrate material or its roughness, which leads to further control of J.

4.4 Summary

Nucleation rates, J, of 2D colloidal crystals on cover glass, Pt-coated cover glass and Au-coated cover glass have been measured. Different J values for each substrate are determined, from which different values of $\Delta\sigma$ are obtained. From the surface force measurements, it is revealed that $\Delta\sigma$ is of relevance to the interaction between particles and substrates. The larger attractive interaction between colloidal particles and substrate yields a higher $\Delta\sigma$ and hence smaller J. We clearly demonstrate that the type of substrate and its roughness are crucial parameters for controlling the nucleation rate of colloidal crystals. Our findings will contribute to extensive applications of colloidal crystals such as in colloidal epitaxy and lithography grown on any substrate.

References

[1] S. X. Guo, J. Nozawa, S. M. Hu, H. Koizumi, J. Okada and S. Uda. Heterogeneous Nucleation of Colloidal Crystals on a Glass Substrate with Depletion Attraction, *Langmuir* **2017**, *33*, 10543−10549.

[2] N. Sato, Y. Aoyama, J. Yamanaka, A. Toyotama and T. Okuzono. Particle Adsorption on Hydrogel Surfaces in Aqueous Media due to van der Waals Attraction, *Sci. Rep.* **2017**, 7: 6099-1–10.

[3] X. Zhang, Y. He, M. L. Sushko, J. Liu, L. L. Luo, J. J. De Yoreo, S. X. Mao, C. M. Wang and K. M. Rosso. Direction-specific van der Waals Attraction between Rutile TiO_2 Nanocrystals, *Science* **2017**, 356, 434–437.

[4] T. Suzuki, Y. W. Zhang, T. Koyama, D. Y. Sasaki and K. Kurihara. Direct Observation of Specific Interaction between Enzyme-substrate Complexes Using Colloidal Probe Atomic Force Microscopy, *Chem. Lett.* **2004**, 33, 5, 536−537.

[5] T. Suzuki, Y. W. Zhang, T. Koyama, D. Y. Sasaki and K. Kurihara. Direct Observation of Substrate-Enzyme Complexation by Surface Forces Measurement, *J. Am. Chem. Soc.* **2006**, *128*, 15209−15214.

[6] J. P. Cleveland and S. Manne. A Nondestructive Method for Determining the Spring Constant of Cantilevers for Scanning Force Microscopy. *Rev. Sci. Instrum.* **1993**, 64 (2), 403–405.

[7] J. N. Israelachivili. Intermolecular and Surface Forces, 2nd ed.; Academic Press: London, **1991**, chapter 11.

[8] J. N. Israelachivili. Intermolecular and Surface Forces, 2nd ed.; Academic Press: London, **1991**. chapter 13.

[9] Ya. I. Rabinovich, B. V. Derjaguin and N. V. Churaev. Direct Measurements of Long-range Surface Forces in Gas and Liquid Media, *Adv. Colloid Interface*

Sci. **1982**, 16, 63−78.

[10] B. V. Derjaguin, Y. I. Rabinovich and N. V. Churaev. Direct Measurement of Molecular Forces, *Nature* **1978**, 272, 313.

[11] H. J. Butt, B. Cappella and M. Kappl. Force measurements with the Atomic Force Microscope: Technique, Interpretation and Applications, *Surf. Sci. Rep.* **2005**, 59, 1–152.

Chapter 5 Conclusion

Though the observation technique and the computational simulation are rapidly developing, the mechanism for revealing the nucleation process is still a challenge due to the limitation of suitable experimental evidence. In this study, colloidal crystals were used as a model for the atomic system to study the mechanism of heterogeneous nucleation on a substrate observed in a single-particle resolution. More importantly, the effect of interfacial energy change, $\Delta\sigma$, was quantitatively evaluated and its origin for colloidal crystals was discussed.

In chapter 1, a general introduction on nucleation and colloidal crystals as a model was presented. The objective of the thesis was also highlighted.

In chapter 2, the principle of colloidal crystallization was introduced. The attractive system driven by depletion attraction was employed for colloidal crystallization to investigate the heterogeneous nucleation on a cover glass substrate. The colloidal particles, polymer, and experimental setup employed in the experiment were described.

In chapter 3, the heterogeneous nucleation of colloidal crystal on a cover glass was discussed. The results are listed as follows:

1. Two types of nucleation processes were found: a cluster that overcomes the critical size for nucleation with a monolayer and a method that occurs with two layers, which is defined as quasi-2D nucleation. This nucleation process is reported for the first time in this study.

2. The number of particles for the critical monolayer and two-layer nuclei at various area fractions on a cover glass, $\phi_{\mathrm{area}}{}^{1}$, was summarized. Throughout the range of $\phi_{\mathrm{area}}{}^{1}$, $N_2{}^{*}$ was less than $N_1{}^{*}$. ΔG for these two types of nucleation processes was evaluated by taking into account the substrate effect.

3. The ΔG calculations suggested that the ΔG of q-2D nucleation was less than that for monolayer nucleation at a given supersaturation. The introduction of $\Delta\sigma$ into ΔG calculation accounts for the occurrence of quasi-2D nucleation.

In chapter 4, the effect of the substrate as interfacial free energy, $\Delta\sigma$, on the nucleation rate of colloidal crystals was investigated. The nucleation processes on uncoated, Au-coated, and Pt-coated cover glass under the same supersaturation were studied. The nucleation rate, J, on the three substrates as a function of ϕ_{area} was measured. The results are summarized as follows:

1. The values of $\Delta\sigma$ on the uncoated, Au-coated, and Pt-coated cover glass were obtained from the CNT equation as 0.83, 1.39, and 1.47 [$k_{\mathrm{B}}T/a^2$], respectively, where k_{B} is the Boltzmann constant, T is the absolute temperature, and a is the particle diameter.

2. The surface force measurements for each substrate were conducted by AFM and the order of the strength of interaction between the particles and substrate was consistent with the order of the magnitude of $\Delta\sigma$ on the three substrates. This indicates that $\Delta\sigma$ is related to the strength of interaction between the particles and substrate, which is the same for the atomic system that $\Delta\sigma$ originates from the bonding energy between the substrate and crystals.

3. The larger the attractive interaction between the colloidal particles and substrate, the higher the $\Delta\sigma$, and hence, the smaller the value of J.

4. The inconsistency of $\Delta\sigma$ determined from J with the prediction by calculation was caused by the roughness of the coated substrate, which was inferred from the result of the surface force measurement.

We have successfully revealed the detailed nucleation process of colloidal crystals on the substrates. Our observations indicate the occurrence of a new

nucleation process: quasi-2D nucleation. This finding significantly impacts the evaluation of the nucleation process. Moreover, the nucleation rate allows us to obtain important parameters, such as $\Delta\sigma$ and γ, through the application of CNT. However, these obtained parameters become inaccurate if quasi-2D nucleation actually occurs.

The pathways in a system are determined through both intermolecular and interparticle interaction and external conditions, such as solution concentration, which provides the amount of chemical potential, and substrate effect, which possibly reduces interfacial free energy. Therefore, more concrete experimental conditions to determine the pathways should be investigated in the future.

The substrate effect, $\Delta\sigma$, was quantitatively evaluated for the nucleation process and was identified to play a crucial role in colloidal nucleation. The magnitude of $\Delta\sigma$ is related to the strength of the interaction between particles and each substrate, which was confirmed via surface force measurements of three different substrates. These findings will contribute to the basic understanding of heterogeneous nucleation on the substrates and to wide fields of colloidal crystal applications, such as colloidal epitaxy and lithography.

List of Achievements

1 Journal Publications:

1. Suxia Guo, Jun Nozawa, Masashi Mizukami, Kazue Kurihara, Akiko Toyotama, Junpei Yamanaka, Hiromasa Niinomi, Junpei Okada, Satoshi Uda, Effect of substrate on nucleation rate of two-dimensional colloidal crystals, Crystals, *Cryst. Growth Des.* **Under review**

2. Jun Nozawa, Satoshi Uda, Suxia Guo, Akiko Toyotama, Junpei Yamanaka, Naoki Ihara, and Junpei Okada, Kink Distance and Binding Energy of Colloidal Crystals, *Cryst. Growth Des.* **2018**, 18, 6078−6083.

3. Jun Nozawa, Satoshi Uda, Suxia Guo, Akiko Toyotama, Junpei Yamanaka, Junpei Okada, and Haruhiko Koizumi, Step Kinetics Dependent on the Kink Generation Mechanism in Colloidal Crystal Growth, *Cryst. Growth Des.* **2018**, 18, 2948−2955.

4. Suxia Guo, Jun Nozawa, Sumeng Hu, Haruhiko Koizumi, Junpei Okada, Satoshi Uda, Heterogeneous nucleation of colloidal crystals on a glass substrate with depletion attraction, *Langmuir* **2017**, 33 (40),10543−10549.

5. Jun Nozawa, Satoshi Uda, Suxia Guo, Sumeng Hu, Akiko Toyotama, Junpei Yamanaka, Junpei Okada, and Haruhiko Koizumi, Two-Dimensional Nucleation on the Terrace of Colloidal Crystals with Added Polymers, *Langmuir* **2017**, 33(13), 3262−3269.

6. 野澤純, 郭素霞, 胡素梦, 豊玉彰子, 山中淳平, 小泉晴比古, 岡田純平, 宇田聡, コロイド結晶における 2 次元核形成過程, *日本結晶成長学会誌*, **2017**, 44(2), 96−102.

7. Sumeng Hu, Jun Nozawa, Suxia Guo, Haruhiko Koizumi, Kozo Fujiwara, and Satoshi Uda, Effect of Solid-Liquid Interface Morphology on Grain Boundary Segregation during Colloidal Polycrystallization, *Cryst. Growth Des.* **2016**, 16(5), 2765−2770.

2 Presentations

(1) Oral presentations in international meetings in Japan:

[1] **2016**/03/18−19; 仙台秋保; 卓越大学院：国際シンポジウム; Two-dimensional nucleation of colloidal crystals doped with polymers; Suxia Guo, Jun Nozawa, Sumeng Hu，Haruhiko Koizumi, Satoshi Uda.

[2] **2017**/03/21−22; 仙台秋保; 卓越大学院：国際シンポジウム; Two dimensional nucleation of colloidal crystals on the substrates with depletion attraction; Suxia Guo, Jun Nozawa, Haruhiko Koizumi, Junpei Okada, Satoshi Uda.

[3] **2018**/03/22−23; 仙台秋保; 卓越大学院：国際シンポジウム; The effect of substrate on nucleation of colloidal crystals; Suxia Guo, Jun Nozawa, Junpei Okada, Satoshi Uda.

(2) Poster presentations in international meetings in Japan:

[1] **2016**/03/18−19; 仙台秋保; 卓越大学院：国際シンポジウム; Two-dimensional nucleation of colloidal crystals doped with polymers; Suxia Guo, Jun Nozawa, Sumeng Hu，Haruhiko Koizumi, Satoshi Uda.

[2] **2017**/03/21−22; 仙台秋保; 卓越大学院：国際シンポジウム; Two

dimensional nucleation of colloidal crystals on the substrates with depletion attraction; Suxia Guo, Jun Nozawa, Haruhiko Koizumi, Junpei Okada, Satoshi Uda.

[3] **2018**/03/22−23; 仙台秋保; 卓越大学院：国際シンポジウム; The effect of substrate on nucleation of colloidal crystals; Suxia Guo, Jun Nozawa, Junpei Okada, Satoshi Uda.

(3) Oral presentations in domestic meetings in Japan:

[1] **2017**/02/17; 宮城県仙台; 東北大学大学院 理学・生命科学 2 研究科合同シンポジウム; Two dimensional nucleation of colloidal crystals on the substrates with depletion attraction; Suxia Guo, Jun Nozawa, Haruhiko Koizumi, Junpei Okada, Satoshi Uda.

[2] **2017**/03/14−17; 神奈川県横浜市; 第 64 回応用物理学会春季学術講演会; In-situ observation of two dimensional nucleation in colloidal crystals with depletion attraction; Suxia Guo, Jun Nozawa, Haruhiko Koizumi, Junpei Okada, Satoshi Uda.

[3] **2017**/06/02−03; 宮城県大崎市; 第 34 回無機・分析化学コロキウム; Two dimensional nucleation of colloidal crystals on a glass substrate via depletion attraction; Suxia Guo, Jun Nozawa, Haruhiko Koizumi, Junpei Okada, Satoshi Uda.

[4] **2017**/11/27−29; 静岡県浜松市; 第 46 回結晶成長会議; Heterogeneous nucleation of colloidal crystals on a glass substrate via depletion attraction; Suxia Guo, Jun Nozawa, Haruhiko Koizumi, Junpei Okada, Satoshi Uda.

[5] **2018**/03/17−20; 東京早稲田大学; 第 65 回応用物理学会春季学術講演会; The effect of substrate on nucleation of colloidal crystals; Suxia Guo, Jun Nozawa, Junpei Okada, Satoshi Uda.

[6] **2018**/10/31−11/02; 宮城県仙台市; 第 47 回結晶成長会議; Effect of

interaction between particles and substrate on nucleation rate of two-dimensional colloidal crystals; Suxia Guo, Jun Nozawa, Masashi Mizukami, Kazue Kurihara, Hiromasa Niinomi, Junpei Okada, Satoshi Uda.

[7] **2019**/03/09−12; 東京東京工業大学; 第 66 回応用物理学会春季学術講演会;Effect of substrate on nucleation rate of two-dimensional colloidal crystals; Suxia Guo, Jun Nozawa, Masashi Mizukami, Kazue Kurihara, Hiromasa Niinomi, Junpei Okada, Satoshi Uda.

(4) Poster presentations in domestic meetings in Japan:

[1] **2016**/11/24; 仙台; 第 132 回東北大学金属材料研究所講演会; In-situ observation of two dimensional nucleation in colloidal crystals with depletion attraction; Suxia Guo, Jun Nozawa, Haruhiko Koizumi, Junpei Okada, Satoshi Uda.

[2] **2017**/02/17; 宮城県仙台; 東北大学大学院 理学・生命科学 2 研究科合同シンポジウム; Two dimensional nucleation of colloidal crystals on the substrates with depletion attraction; Suxia Guo, Jun Nozawa, Haruhiko Koizumi, Junpei Okada, Satoshi Uda.

[3] **2017**/05/26; 仙台; 第 133 回東北大学金属材料研究所講演会; Two dimensional nucleation of colloidal crystals on the substrates with depletion attraction; Suxia Guo, Jun Nozawa, Haruhiko Koizumi, Junpei Okada, Satoshi Uda.

[4] **2018**/05/23; 仙台; 第 135 回東北大学金属材料研究所講演会; The effect of substrate on nucleation of colloidal crystals; Suxia Guo, Jun Nozawa, Junpei Okada, Satoshi Uda.

[5] **2018**/10/29−30; 仙台; 第 136 回東北大学金属材料研究所講演会および Summit of Materials Science 2018; Effect of interaction between particles and substrate on nucleation rate of two-dimensional colloidal crystals; Suxia Guo,

Jun Nozawa, Masashi Mizukami, Kazue Kurihara, Hiromasa Niinomi, Junpei Okada, Satoshi Uda.

Acknowledgements

First, I would like to express my gratitude to my supervisor Prof. Satoshi Uda of the Institute for Materials Research (IMR), Tohoku University. I thank him for giving me the opportunity to be his PhD student after working for three years. I appreciate his invaluable guidance throughout this research as well as the assistance and attention to me. His intelligence, persistence, kindness, patience, profound knowledge, broad vision, and integrity motivated me throughout the research period and will keep driving as I move ahead in life. He is an amazing role model to follow.

Besides my supervisor, I would like to thank my thesis committee, Prof. Tomoteru Fukumura, Prof. Akihide Hibara, Associate Prof. Junpei Okada, for being a part in all my doctoral defense. They devoted their time in reading the thesis and also gave me many valuable suggestions. Thank you very much.

My earnest thanks also go to the Assistant Prof. Jun Nozawa, who introduced me to Colloids and devoted lots of energy and time into the detailed experiment, discussions, as well as the modification for the paper manuscript and this thesis. His enthusiasm for research, serious attitude, kindness, inspiration, and patience also favored the improvement of my presentations and papers.

I am grateful for Dr. Akiko Toyotama and Professor Junpei Yamanaka of Nagoya City University for their helpful discussions and advice. I am thankful to Associate Prof. Masashi Mizukami and Prof. Kazue Kurihara of the Institute of Multidisciplinary Research for Advanced Materials, in Tohoku University, for providing access to the instruments in their laboratory, they helped with the AFM measurement and the suggestion of force data processing. I also extend my profound appreciation to Associate Prof. Hailong Peng, Central South University,

China, for his help in writing the computer program used for counting the particles. I appreciate Minglin Sun, D3, IMR and Dingheng Zheng, D1, IMR for their help in the roughness measurement.

I acknowledge the staffs and members of Uda Laboratory: associate Prof. Junpei Okada of IMR, assistant Prof. Haruhiko Koizumi of IMR (present in the School of Engineering, Nagoya University), assistant Prof. Hiromasa Niinomi of IMR, Dr. Sumeng Hu of North China University of Water Resources and Electric Power, China and Dr. Chihiro Koyama of JAXA, Tsukuba, Japan, for sharing their wisdom and knowledge with me. Thank you very much, Miss Chiharu Nagura, the secretary of Professor Uda's research group, for your numerous assistance.

I wish to thank all the members of Professor Uda's research group: Mr. Qilin Shi, Mr. Bo Peng, Miss Jie Wang, Mr. keiya Sato, Mr. Naoki Ihara, Mr. Yuki Honda, and the graduated students: Mr. Kihyeon Kwon, Mr. Seyoun Choi, Mr. Taqwa Aditya ATMAJA, Mr. Yusuke Horie, Mr.Yutaro Takehara, and Mr. Shuhei Sakano for the study discussions and other fruitful communication. Thanks for the happy working period I spent with you all. I want to take this opportunity to acknowledge some of my best friends in Japan and China: Ying Li, Shuangshuang Zhou and Hailing Xu for their help on different occasions.

I thank the China Scholarship Council (CSC) for the financial support of my doctoral studies in Japan.

Last but not least, I must mention the huge encouragement and support I received from my family during the study period. My husband, Cheng Yang, thank you very much for your love, drive, enormous patience, and constant support all the way, especially sharing the responsibility of looking after our daughter all the time, which all have been a source of strength for me. In particular, many thanks to my daughter, you teach me how to be a mother and bring great joy and a

wonderful time for our family. I am grateful to my parents and family members for giving me their sincere support.

Suxia Guo

January 2019.